ALLOY SUPPORTED SOFC WITH MANGANESE COBALTITE CATHODE

FABRICATION AND CHARACTERIZATION OF ALLOY SUPPORTED SOLID OXIDE FUEL CELL WITH MANGANESE COBALTITE CATHODE

BY

SANJAY KUMAR GUPTA, B.Tech.

A Thesis

Submitted to the School of Graduate Studies

In Partial Fulfillment of the Requirements

For the Degree

Master of Applied Science

McMaster University

Master of Applied science (2005) McMaster University

(Materials Science & Engineering) Hamilton, Ontario

TITLE: Fabrication and Characterization of Alloy Supported Solid Oxide Fuel Cell with Manganese Cobaltite Cathode

AUTHOR: Sanjay Kumar Gupta, B.Tech. (IIT Kanpur, India)

SUPERVISOR: Dr. Anthony Petric

NUMBER OF PAGES: xi, 84

ABSTRACT

This thesis demonstrates two concepts, one a viable fabrication process for an Fe-Cr alloy supported solid oxide fuel cell (SOFC), and second, the use of Co_2MnO_4 (spinel) as the cathode material. Ni/YSZ and YSZ layers were used as anode and electrolyte respectively. The fabrication process consisted of tape casting of iron and chromium oxide powders for the support, dip coating of NiO-YSZ-Fe_3O_4-Cr_2O_3-C and YSZ as anode and electrolyte respectively, synthesis of Co_2MnO_4 from Co_3O_4 and MnO_2 as the , cathode material and finally screen printing of the Co_2MnO_4 cathode. The support, the anode, and the electrolyte were co-fired at 1350°C in air for 10 hours, then Co_2MnO_4 was screen printed and the cell was again fired at 1250°C for 4 hours in air. The complete cell was reduced in pure H_2 at 950°C for 10 hours to convert the major part of support into Fe-Cr alloy, leaving approximately 20% unreduced $FeCr_2O_4$.

The fully fabricated cell was tested at 820°C using 7% H_2, 93% N_2 as the fuel and air as the oxidant. The Co_2MnO_4 cathode which reduced to MnO + Co during the final processing stage was recovered in-situ at the start of the test. Pt mesh was used for current collection. The power density was in the range of 80-120 mW/cm^2.

Acknowledgements

I would like to take this opportunity to express my gratitude for my supervisor Dr. Anthony Petric for his able guidance, generous support, and encouragement. Without his knowledgeable advice, this work could have not been done.

I would also like to extend my sincere thanks to Joshua Deng. He assisted me throughout my research. I have learnt many experimental techniques from him.

I am thankful to Dr. Igor Zhitomirsky for discussing my research work with me. I was able to solve many problems because of his valuable suggestions.

I would like to express a word of thanks for Dr. Rajen Basu, Boris, Ping, Hang, Reza, and Alex for their cheerful friendship and generous help in the laboratory.

Finally, I would like to dedicate my work to my parents for inspiring me for two long years. I was rejuvenated by their never diminishing inspiration.

TABLE OF CONTENTS

LIST OF FIGURES

LIST OF TABLES

CHAPTER 1

INTRODUCTION

Fuel cells are continuously fuelled electrochemical power sources. They are more efficient, less polluting, and quieter than other power generation systems. Successful implementation of this technology will ensure a supply of clean energy and will help to alleviate problems caused by environmental degradation. Among the various types, solid oxide fuel cells (SOFCs) are the most efficient and have highest operating temperature (600-1000°C). When the SOFC is coupled with a gas turbine, the overall efficiency could reach 75%. Any type of hydrocarbon fuel can be used. An SOFC stack consists of layers of cathode, electrolyte, anode, and interconnect. SOFCs can be fabricated in various sizes and shapes and this further broadens their application area.

Many materials have been investigated for SOFC components of which the most popular are Ni/YSZ as the anode, YSZ as the electrolyte, and LSM as the cathode. The anode supported SOFC yields the maximum power output in comparison with electrolyte-supported cells. The anode supported cells consist of thin layers of the cathode and the electrolyte (<50 micron) on a thick (0.4-2.0 mm) Ni/YSZ support. The SOFC design has certain drawbacks and the present work is an attempt to address two of them.

While the cell is in operation, Ni/YSZ is exposed to reducing atmosphere but when the fuel is shut off, Ni can quickly oxidize to NiO. This process is repeated every time cell is turned on and off. Continued oxidation and reduction cycling makes the Ni/YSZ support more friable until it ultimately disintegrates.

In the present work, the support layer has been changed to an Fe-Cr alloy that,unlike Ni, will be resistant to redox cycling. Therefore, the rate of degradation of the anode will be greatly reduced. Visco et al. [2, 3] have demonstrated the concept of fabrication of an Fe-Cr support starting with stainless steel powder and processing in a controlled atmosphere. In the present work, Fe_3O_4 and Cr_2O_3 powders were the starting materials and the processing was done in air. Finally, the complete cell was reduced in H_2 at 950°C for 10 hours to convert the oxides into alloy.

Another problem arises with the conventional LSM cathode material during the fabrication stage; pyrochlore ($La_2Zr_2O_7$) or perovskite phases ($SrZrO_3$) are formed at the cathode-electrolyte interface. These phases are insulating and lead to greatly decreased cell performance. Co_2MnO_4 has good electronic conductivity and matching thermal expansion with other cell components. This spinel compound does not react with zirconia to form the pyrochlore phase. Therefore, this material could be used as a promising candidate for the SOFC cathode.

The next chapter describes the concept and current status of SOFCs. The fabrication technique of alloy-supported SOFCs with spinel material as cathode is described in chapter three. Chapter four deals with the microstructural, compositional, and performance analysis of the fabricated cell. The fabrication process and performance output results are compiled with suggestions for possible improvements in chapter five. Some useful results for an alternate fabrication process are compiled in the appendix.

CHAPTER 2
LITERATURE REVIEW

2.1 Fuel Cells

A fuel cell is an energy conversion device that converts the chemical energy of a fuel gas directly to electrical energy and heat without the need for flame combustion as an intermediate step, giving much higher conversion efficiencies than conventional thermo-mechanical methods.

2.1.1 Types of Fuel Cells

The various types of fuel cells are named after the type of electrolyte employed.

2.1.1.1 Alkaline Fuel Cell (AFC)

The Alkaline Fuel Cell system had an important role in the historical development of fuel cells. Bacon used this system to construct the first practical fuel cell in which he obtained 230 mA/cm^2 at 0.8 V [4] in 1953. The AFC has the advantage of high solubility of molecular oxygen in alkaline electrolyte leading to higher oxygen reduction. A major disadvantage is that the KOH electrolyte reacts with CO_2 impurities in the fuels that in turn degrade the cell performance.

2.1.1.2 Polymer Electrolyte Membrane Fuel Cell (PEM)

It is thought that for most applications fuel cells will be supplied with hydrocarbon fuels and there is a need to avoid the problem of reaction of electrolyte with CO_2. PEM fuel cells are one of the solutions to this problem. PEM fuel cells are particularly appropriate for electric vehicles and as a replacement for batteries for

portable and mobile applications such as mobile telephones, laptop computers, and the electronic equipment carried by military personnel [4].

2.1.1.3 Direct Methanol Fuel Cell (DMFC)

Most of the research on Direct Methanol Fuel Cells is based on a sulphuric acid electrolyte, but more recent work has focused on the Nafion polymer electrolyte membrane. A major problem with the Nafion membrane is its permeability to methanol which lowers effective fuel utilization, and degrades the performance of the cathode. The work on DMFC systems clearly demonstrates the need for an alternate polymeric electrolyte to Nafion with minimal methanol permeability, and higher temperature operation.

2.1.1.4 Phosphoric Acid Fuel Cell (PAFC)

The other CO_2 tolerant low temperature system is the Phosphoric Acid Fuel Cell operating at 200°C. The gas distribution plates consist of two ribbed porous graphite substrates which also serve as electrolyte reservoirs, together with another dense impermeable graphite sheet which functions as a bi-polar separator plate. These graphite components are relatively expensive to manufacture and restrict the operational window of the cells.

2.1.1.5 Molten Carbonate Fuel Cell (MCFC)

MCFC systems were originally conceived as large (gigawatt scale) centralized coal fired power plants. The biggest problem with this type of cell is management of the electrolyte. Control of the optimal composition of molten carbonate is critical for achieving high performance and longevity for MCFC systems, However various

processes, including corrosion reactions, voltage driven migration, creepage and vaporization of the molten salt, all tend to contribute to the redistribution of the electrolyte, and subsequent degradation of stack performance and longevity [4].

2.1.1.6 Solid Oxide Fuel Cell (SOFC)

This new generation of fuel cells consists of solid ceramic electrolyte and electrodes and offers the possibility of use in stationary as well as in mobile applications without the need for electrolyte management. Since this thesis is based on the fabrication and processing of SOFC components all the aspects of this type of fuel cell will be discussed in subsequent sections.

There are also other types of fuel cells which are less employed, but may later find a specific application. Examples are air-depolarized cells, sodium amalgam cells, biochemical fuel cells, inorganic redox cells, regenerative cells, alkali metal-halogen cells, etc. [5]. Technical characteristics of the major types of fuel cell are listed in the table 2.1.1.6

Table 2.1.1.6 Operational characteristics of important types of fuel cell [5]

Types of fuel Cell	Electrolyte	Operating Temperature(°C)	Fuel	Oxidant	Efficiency (%)
AFC	potassium hydroxide	50-200	pure hydrogen, or hydrazine	O_2/Air	50-55
DMFC	polymer	60-200	liquid methanol	O_2/Air	40-55
PAFC	phosphoric acid	160-210	hydrogen from hydrocarbons	O_2/Air	40-50
PEM	polymer, proton exchange membrane	50-80	less pure hydrogen from hydrocarbons or methanol	O_2/Air	40-50
MCFC	molten salts such as potassium carbonate, lithium carbonate	630-650	hydrogen, carbon monoxide, natural gas, propane, marine diesel	O_2/Air/CO_2	50-60
SOFC	ceramic such as stabilized zirconia and doped pervoskite or fluorite	600-1000	hydrocarbons	O_2/Air	45-60

2.1.2 Historical Perspective of Fuel Cells

Despite their modern high-tech aura, fuel cells actually have been known to science for more than 160 years and became the subject of intense research and development, especially since World War II. Alessandro Volta (1745-1837) was the first scientist to place the observations of the theoretical phenomena on a scientific footing. J.W. Ritter (1776-1810), also known as the founder of electrochemistry, continued to develop the understanding of electricity. Sir Humphrey Davy created, in 1802, a simple

fuel cell based upon a compound (C/H_2O, $NH_3/O_2/C$) delivering a feeble electric shock. The discovery of the fuel cell principle is credited to Christian Friedrich Schonbein in 1838. Sir William Grove (1811-1896), an English lawyer turned scientist, won renown for his development of an improved wet cell battery in 1839, the 'Grove Cell', as it came to be called. This cell type is based on reversing the electrolysis of water [5]. Ceramic fuel cells came much later and began with Nernst's discovery of solid oxide electrolytes in 1899.

Freidrich Wilhelm Ostwald (1853-1932), a founder of the field of physical chemistry, provided much of the theoretical understanding of how fuel cells operate. Emil Baur (1873-1944) of Switzerland conducted wide-ranging research into different types of fuel cells during the first half of 20^{th} century. Baur's work included high temperature devices (using molten silver as an electrolyte) and a unit that used a solid electrolyte of clay and metal oxides [5].

Francis Thomas Bacon (1904-1992) began researching alkali electrolyte fuel cells in the 1930s. In 1939, his first cell was built. Since 1945, three research groups (US, Germany, and the former USSR) undertook studies on some principal types of generators by improving their technologies for industrial development purposes. These studies yielded the actual concepts, later used at Siemens, and Pratt & Whitney. In connection with the Apollo space program in 1960, NASA embarked on a successful program that used hydrogen-based fuel cells to power the on-board electrical systems on the Apollo journey to the moon.

Beginning in the mid-1980s government agencies in the US, Canada and Japan significantly increased their funding for fuel cell R&D.

Fuel cells were first used in spaceflight (Gemini spacecraft, Skylab, Space Shuttle), and make sense for transportation, portable power, home power generation and large scale power generation [5].

2.2 Solid Oxide Fuel Cells (SOFCs)

SOFCs have recently emerged as a serious application for high temperature fuel cell technology. They promise to be extremely useful in large, high-power applications such as full scale industrial stations and large-scale electricity-generating stations. Some fuel cell developers propose SOFCs for uses in motor vehicles. An SOFC system usually utilizes a solid ceramic as the electrolyte and operates at high temperatures (600-1000°C). This high operating temperature allows internal reforming, promotes rapid electro-catalysis with non-precious metals, and produces high quality byproduct heat for cogeneration. Efficiencies for this type of fuel cell can reach up to 70% with an additional 20% as heat recovery [5].

2.2.1 SOFC Stack Components

An SOFC single cell consists of an oxide electrolyte sandwiched between an anode and a cathode. Under typical operating conditions (with hydrogen fuel and oxygen oxidant), a single cell produces less than 1 V. Thus, practical SOFCs are not operated as single units; rather, they are connected in electrical series to build voltage. A series of cells is referred to as a stack. A component variously called an interconnect or bipolar separator, connects the anode of one cell to the cathode of the next in a stack. The

principal components of an SOFC stack are the electrolyte, the anode, the cathode, and the interconnect [1]. SOFCs are fabricated in various geometries such as tubular, [13], segmented-cell-in series, and flat-plate (planar) [1]. Present work is focused on the planar SOFC which is shown below in fig. 2.1

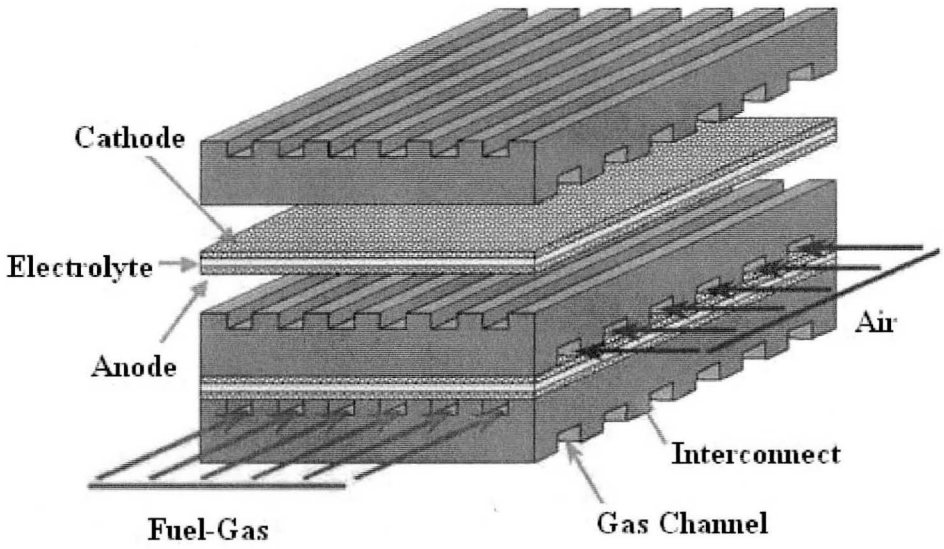

Figure 2.1 SOFC components (Expanded view) [7]

2.2.2 Fuel Cell Power System (Auxiliary Units)

In an SOFC power plant, besides cell stacks, pumps, heat exchangers, fuel processing units, and ducting are required, normally referred to as balance-of-plant (BOP). To ensure stable electrical output to an external load requires appropriate DC/AC invertors and system control for the stack. [4] A schematic of a fuel cell assembly is shown in fig. 2.2 below.

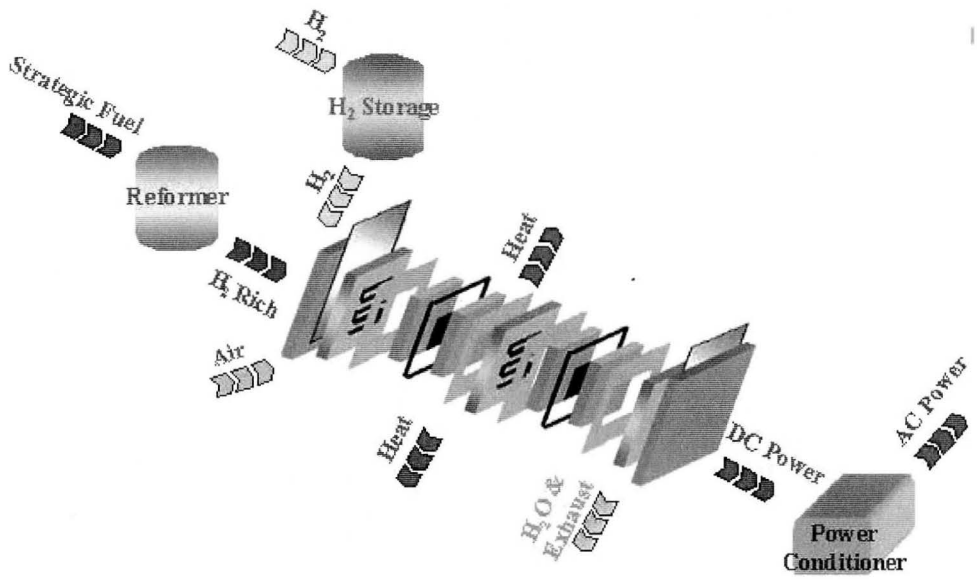

Figure 2.2 Schematic view of PEM with BOP [8]

2.2.3 Principles of Operation

2.2.3.1 Electrical Conduction in Electrolytes and Electrodes

Fluorite-type oxides are commonly ionic conductors and have been considered for use as electrolytes in SOFCs. The fluorite structure (CaF_2) is adopted by a number of oxides of the general formula MO_2, where M is a large tetravalent cation. The unit cell of the fluorite-type oxide has the so-called M_4O_8 structure. This structure is schematically shown in fig. 2.3

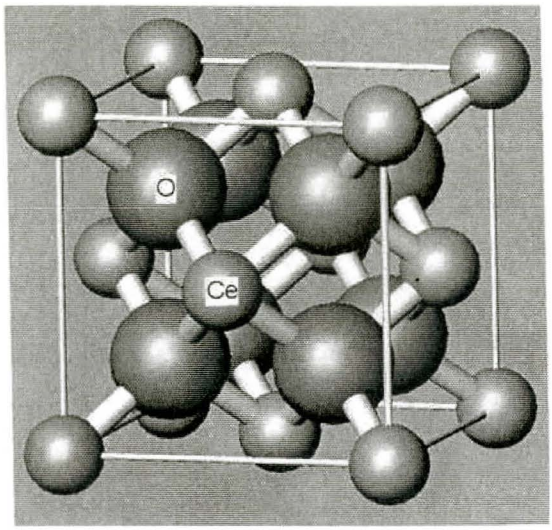

Figure 2.3 Fluorite type crystal structure [12]

In this fluorite structure, each metal ion is surrounded by eight oxygen ions, forming a body-centered cubic structure. To form the fluorite structure in MO_2, the limiting (minimum) ionic radius ratio (the ratio of metal-ion radius to oxygen-ion radius) is 0.732 [1].

Under normal conditions of temperature and pressure, certain MO_2 oxides do not have the fluorite structure because the ionic radius ratio condition is not satisfied; one example is ZrO_2. At room temperature, ZrO_2 has a monoclinic crystal structure, which is a distorted form of fluorite. The monoclinic structure changes to tetragonal form above 1170°C. The fluorite structure only exists at temperatures above 2370°C. However, the addition of certain aliovalent cations stabilizes the fluorite structure of ZrO_2 from near room temperature to its melting point of 2680°C. The fluorite structure of ZrO_2 is stabilized by direct substitution of divalent or trivalent cations of appropriate size for the host lattice cation Zr^{4+}. In this case, lattice defects are created to preserve the electroneutrality condition in the solid solution. The presence of a high oxygen-vacancy

concentration in stabilized ZrO_2 gives rise to high oxygen-ion mobility, resulting in high oxygen ion conductivity. Oxygen ion conduction takes place in stabilized ZrO_2 by movement of oxygen ions via vacancies [1].

Oxides of the general formula ABO_3 (A is a large divalent or trivalent cation and B is a tetravalent or trivalent transition metal cation) belong to the class of compounds having the perovskite structure. A large number of perovskite oxides have orthorhombic, rhombohedral, or tetragonal structures which can be considered as distortions from the ideal cubic form. A schematic diagram of the perovskite crystal structure is shown in fig. 2.4. The rare earth perovskite oxides are commonly used as cathode and interconnect materials for ceramic fuel cells.

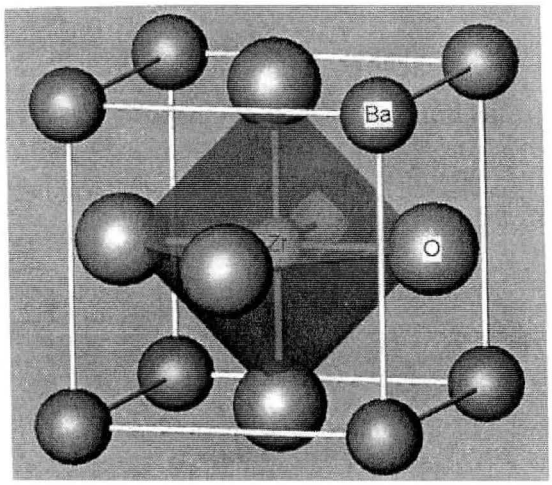

Figure 2.4 Perovskite type crystal structure [12]

2.2.3.2 Mechanism

The operation of a fuel cell involves the reduction of the oxidant at the cathode and the oxidation of the fuel at the anode. The common fuel and oxidant for testing SOFCs

are hydrogen and air respectively. Thus, the reactions in the SOFC involve the oxidation of hydrogen and reduction of oxygen at the electrodes [1]. This operation is schematically shown for oxygen ion conducting electrolyte in fig. 2.5.

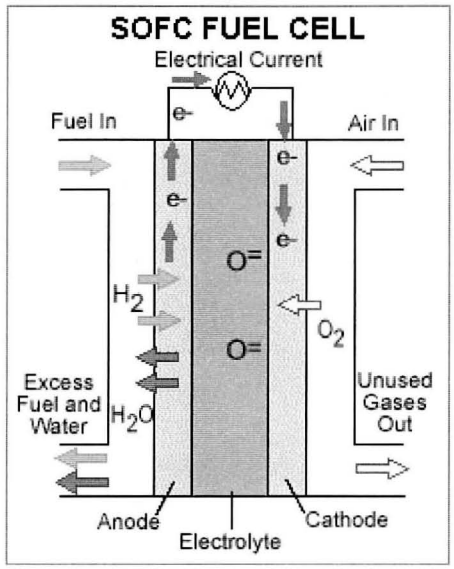

Figure 2.5 Schematic of operation of oxygen ion conducting SOFC [6]

2.2.3.3 Thermodynamic Principles

For an oxygen ion-conducting electrolyte, reduction of oxygen occurs at the cathode of the SOFC

$$O_{2(c)} + 4e^- = 2O^{2-}{}_{(e)} \qquad \text{(Eq 1)}$$

where subscripts (c) and (e) refer to the cathode and electrolyte respectively. At the anode reduction of oxygen ions takes place as

$$2O^{2-}{}_{(e)} = O_{2(a)} + 4e^- \qquad \text{(Eq 2)}$$

where the subscript (a) refers to the anode. Therefore the overall cell reaction can be written in the following way.

$O_{2\,(c)} = O_{2\,(a)}$ (Eq. 3)

Eq. 3 reflects that the SOFC can be considered as an oxygen concentration cell and therefore the reversible (thermodynamic) cell voltage would be given by the Nernst equation.

$$E_r = \frac{RT}{4F} \ln \frac{PO_2(c)}{PO_2(a)} \quad \text{(Eq 4)}$$

Here R is universal gas constant. T is temperature, F is the faraday constant, and PO_2 is the partial pressure of oxygen at the electrodes [1].

2.2.3.4 Thermodynamic Efficiency

A simplified way to illustrate the efficiency of an energy conversion device is to examine the theoretical maximum efficiency. The efficiency limit for heat engines such as steam and gas turbines is defined by the Carnot cycle as the maximum efficiency = $(T_1-T_2)/T_1$, where T_1 is the maximum temperature of the fluid in the heat engine, and T_2 is the temperature at which the heated fluid is released. All temperatures are in Kelvin, and therefore the lower temperature T_2 is never small (Usually > 290 K). Electrical energy generation in heat engines involves thermal end mechanical losses at intermediate combustion step. This affects the overall efficiency of heat engines.

For fuel cells, the situation is very different. Fuel cell operation is an electro-chemical process, such as hydrogen oxidation to produce water, and thus involves the

changes in Gibbs free energy (ΔG). It is the change in Gibbs free energy of formation that is converted to electrical energy.

The maximum efficiency for a fuel cell can be directly calculated from ΔG and ΔH as = ΔG/ (-ΔH). The ΔH value for the reaction is different depending on whether the product water is in its vapor or liquid state. If water is liquid, then (-ΔH) is higher due to release of heat of condensation. The higher value is called higher heating value (HHV), and the lower value is called lower heating value (LHV) [10]. Jacob et al. [9] have shown a refined definition of efficiency, which is $\Delta G/(\Delta H + q)$, where q is the heat exchanged by the cell with the surroundings. In the revised definition, the maximum thermodynamic efficiency cannot be greater than one.

2.2.4 SOFC Advantages

SOFCs are more efficient electricity generators than conventional heat engines. When hybrid systems are employed, the overall efficiency could reach 70% to 90% [5, 10]. Therefore this technology is very suitable for applications in the distributed generation market (i.e. stationary power) because its high conversion efficiency provides the greatest benefits when fuel costs are higher.

SOFCs are flexible in terms of fuel choice such as carbon based fuels, e.g., natural gas. Besides the choice in fuel selection, they are flexible in terms of geometry. They have modular and solid state construction without moving parts, therefore quiet enough to be installed indoors [5, 24].

The high operating temperature of SOFCs produces high quality byproduct heat which can be used for co-generation or for use in combined cycle applications. The solid

electrolyte avoids electrolyte management problems, for example, the problems of handling and corrosion as in the case of liquid electrolyte. SOFCs have the potential for a deep impact on improving the environment.

Table 2.2 shows global CO_2 emissions of the top fifteen nations per capita (tonnes) [5]

Table 2.2 Global CO_2 emissions of the top fifteen nations per capita (tonnes) [5]

Rank	Nation	CO_2	Rank	Nation	CO_2	Rank	Nation	CO_2
1	USA	19.1	6	UK	10.1	11	France	6.3
2	Russia	18.0	7	Japan	8.8	12	S. Korea	5.8
3	Australia	14.4	8	Poland	7.7	13	Mexico	3.6
4	Canada	13.9	9	Italy	7.1	14	China	2.1
5	Germany	12.2	10	S. Africa	7.1	15	India	0.8

Table 2.3 Typical SOFCs emissions from one year of operation in comparison to fossil fuels [5]

Air emissions*	SO_x	NO_x	CO	Particles	Organic Compounds	CO_2
Fossil Fuelled Plant	12,740	18,850	12,797	228	213	1,840,020
SOFC system	0	0	32	0	0	846,300

* kg of emissions per 1650 MWH from one year full operation

Table 2.3 shows that by using SOFC systems, we can get extremely low emissions by eliminating the danger of carbon monoxide in exhaust gases, as any CO

produced is converted to CO_2 at the high temperature. Total CO_2 emission is half an order of magnitude less than the emission of conventional fossil fuel fired plants. By estimating the total CO_2 emission of the world (as is given for top fifteen countries according to their CO_2 emissions per capita) we can solve environmental problems caused by green house effect.

SOFCs have a potential long life expectancy in the range of 40,000-80,000 h [5].

2.2.5 SOFC Disadvantages

The high operating temperature of SOFCs is advantageous for the processing of common fuels and for combined SOFC/gas-turbine power plants. On the other hand, significant disadvantages concerning the long-term stability and costs of materials and components as well as the demand for a short start up time for mobile applications arise.

The operating temperature of SOFCs is restricted by thermally activated transport processes and electrochemical reactions such as oxygen ion conductivity of the solid electrolyte and different reactions steps in the electrodes, and at the electrode /electrolyte interfaces.

Decreasing the operating temperature generally results in decreased power density and/or efficiency. On the other hand, the long term stability of the system can be improved and the system costs reduced by using less costly metal alloys for interconnects and external components [23].

Dynamic operation, i.e., fast startup, loads and thermal cycling as well as redox-cycles due to gas supply failures are still unsolved problems [23].

Hydrogen fuel is not readily available and thus on-site or on-board H_2 production via reforming is necessary. There are no readily available and affordable ways for on-board or on-site desulphurization of hydrocarbon fuels and this presents a challenge for using hydrocarbons fuels [10].

2.2.6 Future Trends

A very recent development in solid oxide fuel cells is the demonstration of single chamber fuel cells (SCFCs). Such cells, fig. 2.6, utilize mixed fuel/oxidant mixtures in a single gas inlet and rely on carefully selected anode and cathode catalysts to produce well-controlled, half-cell reactions:

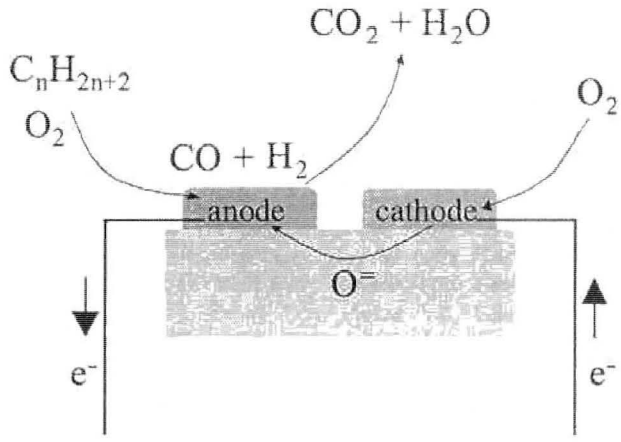

Figure 2.6 Schematic operation of SCFC [4]

At anode: $CH_4 + 1/2O_2 = CO + 2H_2$

$H_2 + O^{=} = H_2O + 2e^{-}$ (electrochemical)

$CO + O^{=} = CO_2 + 2e^{-}$ (electrochemical)

At cathode: $1/2\ O_2 + 2e^- = O^=$ (electrochemical)

Ideally, simple chemical oxidation of the hydrocarbon, which would yield CO_2 and H_2O, does not take place. Instead, partial oxidation occurs at the anode and the products of this reaction are then consumed electrochemically, while oxygen is consumed electrochemically at the cathode. Because complications due to sealing are eliminated, the SCFC greatly simplifies system design and enhances thermal and mechanical shock resistance, thereby allowing rapid startup and cool down. While it may seem optimistic, at first glance, to expect that catalysts could be sufficiently selective so as to yield good power densities, such chemical precision is utilized in nature. Indeed, biofuel cells operating on aqueous glucose that is not separated from ambient oxygen demonstrate essentially perfect electrode selectivity and may ultimately enable extremely compact fuel cell designs that are ideally suited to miniature, low power applications [12].

2.3 Materials Consideration of SOFC Components

2.3.1 Anode

The prime function that anode serves in SOFC is to provide reaction sites for the electrochemical oxidation of the fuel. This function requires some stringent requirements from the materials point of view. Anode material should have stability (chemical, phase, morphological, and dimensional) in the fuel reducing environment and have sufficient electronic conductivity and catalytic activity for the fuel gas reaction in operating conditions [1]. It should have matching thermal expansion to other components to avoid cracking and should have sufficient porosity to allow gas transport to the reaction sites. It should have good fabricability and adequate mechanical strength [5]

Promising materials for anode applications are composite mixtures of the electrolyte material with transition metal elements (Ni, Co, Ru). Alternatively, mixed conducting oxides have also been investigated as SOFC anode materials. In mixed conductors in which both oxygen ions and electrons are mobile, the electrochemical reactions occur over the entire electrode/gas interfacial area (triple phase boundary, TPB). ZrO_2-Y_2O_3-TiO_2 solid solutions are of particular interest in this category [1]. Rare earth doped CeO_2 is a viable anode material for an intermediate temperature solid oxide fuel cell due to its advantageously high electrocatalytic activity that enables the direct oxidation of low hydrocarbon gases. Unfortunately, the occurrence of pronounced ionic conductivity along with mechanical degradation in reducing atmospheres poses a great concern for its practical application [20].

Porous Ni/YSZ cermet (YSZ: yttria stabilized zirconia) is currently the most common anode material for SOFC applications because of its low cost. It is also chemically stable in reducing atmospheres at high temperatures and its thermal expansion coefficient is close to that of the YSZ-electrolyte. More importantly, the intrinsic charge transfer resistance that is associated with the electrocatalytic activity at Ni/YSZ boundary is low. More than 30%, by volume, of continuous porosity is required to facilitate the transport of reactant and product gases. Nickel serves as an excellent reforming catalyst and electrocatalyst for electrochemical oxidation of hydrogen. It also provides predominant electronic conductivity for the anode. The YSZ constitutes a framework for the dispersion of Ni particles and acts as an inhibitor for the coarsening of Ni powder during both consolidation and operation. Additionally, it offers a significant part of ionic

contribution to the overall conductivity, thus effectively broadening the three-phase boundaries. Finally the thermal expansion coefficient of the anode can be tailored to match the other SOFC components as YSZ is mixed with Ni in an arbitrary ratio [20].

Besides the inherent properties of Ni, the fabrication process is very important to keep overall anode resistance low. The electrical resistance of the anode is essentially composed of internal resistance, contact resistance, concentration polarization resistance, and activation polarization resistance. The internal resistance refers to resistance to the transport of electrons within the anode, and therefore, is determined by the magnitude of electronic resistivity and thickness of anode. The contact resistance is caused by poor adherence between anode and electrolyte. Concentration polarization is related to the transport of gaseous species through the porous electrodes and, thus, its magnitude is dictated by the microstructure of the electrode, specifically, the volume percent porosity, the pore size, and the tortuosity factor. Activation polarization is related to the charge transfer processes and depends on the area of electrode/electrolyte/ gas triple-phase boundaries (TPB) and the electrocatalytic activity of the electrode itself. It is proposed that for an optimum performance of the cell, the Ni content in the anode should fall between 40-50 volume percent [16, 17, and 20] and YSZ particles should have a broad particle size range. It has been observed that smaller NiO and larger YSZ powder showed the best anodic performance on aspects of initial activity and long-term stability [15, 20].

It is well established that the major mechanism of anode performance degradation is either Ni coarsening or agglomeration after long-term operation, leading to a reduction in both the TPB and electrical conductivity. Aside from being prone to coarsening at

operating temperatures, poor carbon and sulfur resistances are the other two prominent drawbacks of Ni/ZrO_2 anode cermet. Nickel is an excellent electrocatalyst for electrochemical oxidation of hydrogen. However, this activity is impaired when the natural gas or methane is directly used as fuel due to carbon deposition. Formation of carbon deposits on Ni particles is responsible for excessively high activation polarization, which leads to the rapid deterioration of cell performance [20]. Koh et al. [18] have observed that carbon deposition by humidified methane is reversible when it is oxidized at a current load of thermodynamically carbon-free condition and this reversible carbon deposition does not affect cell performance. On the other hand, irreversible carbon formation occurs with dry methane fuel at thermodynamically carbon-favored condition, and this irreversible carbon particulate is the main reason for cell performance degradation.

Low sulfur tolerance of the Ni/YSZ anode constitutes another hurdle to the use of natural gas as fuel. The deactivation from sulfur poisoning occurs because H_2S strongly absorbs on active sites of nickel, leading to the substantial reduction in the rate of electrochemical reaction occurring at TPBs [20]. The poisoning effect has been found to have a large dependence on the operating temperature, which requires that, a high grade desulfurization process will be necessary for reducing the operating temperature [22]. Mukundan et al. [19] have observed that perovskite-based anodes (as LSCM/YSZ etc.) offer at least an order of magnitude improvement in sulfur tolerance over the Ni/YSZ anodes.

As a note of caution, raw material should not have impurities of SiO_2 or Na_2O as these impurities segregate from the bulk and accumulate at the anode/electrolyte interface along the three-phase boundaries. This ultimately leads to degraded cell performance [21].

2.3.2 Cathode

The purpose of the cathode in the fuel cell is to provide reaction sites for the electrochemical reduction of the oxidant. Therefore, requirements for the cathode materials and structures are the same as those of anodes except that the cathode must be stable in the oxidizing environment and have sufficient electronic conductivity and catalytic activity for the oxidant gas reaction under operating conditions [1].

Pervoskite type lanthanum strontium manganite, La(Sr)MnO_3 (LSM) and lanthanum calcium manganite, La(Ca)MnO_3 (LCM) offer excellent thermal expansion match with zirconia electrolytes and provide good performance at operating temperatures above 800°C. For applications requiring lower temperature operation (600-800°C), a range of alternative perovskite-structured ceramic electrode materials are available. These include lanthanum strontium ferrite (LSF), (La, Sr)(Fe)O_3, lanthanum strontium cobaltite (LSC), (La, Sr)CoO_3[30], lanthanum strontium cobaltite ferrite (LSCF), (La, Sr)(Co, Fe)O_3, lanthanum strontium manganite ferrite (LSMF), (La, Sr)(Mn, Fe)O_3, samarium strontium cobaltite (SSC), (Sm, Sr)CoO_3, lanthanum calcium cobaltite ferrite (LCCF), (La, Ca)(Co, Fe)O_3, praseodymium strontium manganite (PSM), (Pr, Sr)MnO_3, and praseodymium strontium manganite ferrite (PSMF), (Pr, Sr)(Mn, Fe)O_3. Usually perovskite electrode materials are mixed with electrolyte materials to improve

performance [5].Other possible candidates for cathode materials for intermediate temperature operation are Ce doped $SrMnO_3$ [25] and $Gd_{1-x}Sr_xMnO_3$ ($0 \leq x \geq 0.6$) [26]. Murray et. al. [28] have observed that the performance of LSCF cathodes could be improved by addition of a gadolinium doped ceria second phase.

Among others, LSM is widely used as the cathode material for SOFC applications. Lanthanum manganite is a p-type perovskite oxide and shows reversible oxidation-reduction behavior. The material can have oxygen excess or deficiency depending upon the ambient oxygen partial pressure and temperature. Although, it is stable in air and oxidizing atmospheres, it dissociates at 1000°C at oxygen pressures $\leq 10^{-14}$ atm. The electronic conductivity of lanthanum manganite is due to hopping of an electron hole between the +3 and +4 valence state of Mn. This conductivity is enhanced by doping with a divalent ion such as calcium or strontium.

It has been observed that during cell operation, the cathode accounts for the major portion of polarization losses [23]. This loss can be minimized by choosing an appropriate composition and by adjusting the microstructure. For example, to increase the cathode performance, the number of active reaction sites has to be increased. This may be achieved by using a composite electrode consisting of an LSM/YSZ-composite. The limitations of a composite electrode is the arbitrary distribution of the LSM and YSZ-particles. Therefore, only a part of the electrode volume is active for oxygen reduction. A well defined increase of the effective electrolyte surface area can be achieved by a structured electrolyte surface [53].

Use of LSM with YSZ has some unsolved problems. First of all is the formation of insulating phases during the fabrication stage of the cell. The formation of compounds $La_2Zr_2O_7$ and $SrZrO_3$ usually takes place above 1100°C. The mechanism of formation can be understood as follows. La and Mn diffuse into YSZ and a solid solution of YSZ with La and Mn is formed. The formation of a reaction product La2Zr2O7 originates from the difference of the solubility limit of La and Mn in YSZ. By the diffusion of Mn into YSZ, La_2O_3 is formed. This La_2O_3 reacts with YSZ to form $La_2Zr_2O_7$. The oxygen ion conductivity of $La_2Zr_2O_7$ is of the order of 10^{-4} S cm^{-1} at 1000°C [29], which is three orders lower than that of 8YSZ (10^{-1} S cm^{-1}). Besides this, its thermal expansion coefficient mismatch with electrolyte and cathode causes cracks and gas leaks. Therefore, its presence at the interface is undesirable [29]. At high Sr concentration the predominant product is $SrZrO_3$ [27], also an insulating phase.

Another problem is popularly termed as "chromium poisoning". This problem occurs in conjunction with Cr containing interconnect materials, and during operation several types of Cr species are observed in regions where the cathode, electrolyte, and oxygen gas all come together at common locations. Because this triple-phase boundary (TPB) is located hundreds or even thousands of micrometers away from the metal interconnect, it is generally recognized that the high oxygen environment of the cathode compartment leads to the formation of volatile Cr (VI) oxides and oxyhydroxides from the protective Cr_2O_3-containing film on the metal interconnect [24]. These species then diffuse throughout cathode compartment where they can re-equilibrate to deposit solid Cr_2O_3. This would be expected to occur most readily in regions where there is low

oxygen partial pressure, a reducing environment, and the means to remove electro-generated oxygen anions (O^{2-}). Because the highest rate of oxygen consumption occurs at the TPB of an active cathode, with concurrent production of oxygen anions (O^{2-}), it would be logical to assume that the highest concentration of deposited Cr_2O_3 would be at the TPB. Not only would this reaction compete with the electrochemical reduction of oxygen, but it would also result in the deposition of solid species that could block further reduction of oxygen gas at these sites [12, 31, and 56]

Fujita et. al.[32] have observed that LSCO coating on Cr-containing alloy was very effective in reducing the growth of Cr_2O_3 on the Cr-containing alloys, this in turn reduced Cr-poisoning of the cathode and therefore stack voltage degradation rate was low.

2.3.3 Electrolyte

The SOFC electrolyte conducts ions between the anode and cathode. The electrolyte transfers the ions produced at one electrode to the other electrode to balance the charge from the electron flow and complete the electrical circuit in the fuel cell. The electrolyte also separates the fuel from the oxidant in the fuel cell. Thus, the electrolyte material must be stable in both reducing and oxidizing environments, impermeable to the reacting gases, and sufficiently conductive (ionically) at the operating conditions. Since the SOFC operates at high temperatures (600-1000°C), the electrolyte must be chemically and thermally compatible with the other cell components from room temperature to the operating temperature, and to even higher temperatures at which fuel cell is fabricated [1].

The most popular materials for the SOFC electrolyte are cerium oxide doped with samarium (SDC), $(Ce_{0.85}Sm_{0.15})O_{1.925}$; cerium oxide doped with gadolinium (GDC), $(Ce_{0.90}Gd_{0.10})O_{1.95}$; cerium oxide doped with yttrium (YDC), $(Ce_{0.85}Y_{0.15})O_{1.925}$; cerium doped with calcium (CDC), $(Ce_{0.88}Ca_{0.12})O_{1.88}$; lanthanum strontium gallium magnesium (LSGM), $(La_{0.80}Sr_{0.20})(Ga_{0.90}Mg_{0.10})O_{2.85}$ or $(La_{0.80}Sr_{0.20})(Ga_{0.80}Mg_{0.20})O_{2.80}$; bismuth yttrium oxide (BYO), $(Bi_{0.75}Y_{0.25})_2O_3$; barium cerate (BYC), $(Ba_{0.75}Y_{0.25})_2O_3$;strontium cerate (SYC), $Sr(Ce_{0.95}Yb_{0.05})O_3$ [5]

Ce-based oxide ion conductors offer a significantly higher ionic conductivity but they become mixed conductors in the anode environment resulting in an internal short circuit of the cell. Therefore, a decreased open circuit voltage (OCV) and additional fuel utilization even under OCV-condtions takes place resulting in decreased system efficiency [23, 35, and 53].

The ion transport properties of bismuth oxide have received significant academic attention as a result of a rather spectacular phase transition at ~700°C which leads to an increase in conductivity by almost three orders of magnitude. In the high temperature δ phase, the compound has a cubic fluorite structure, with an extremely high (25%) oxygen vacancy content. Below the transition, the vacancies are ordered, and hence have low conductivity. The key limitations of bismuth based compounds are their very high electronic conductivities, and tendencies to become reduced to bismuth metal in hydrogen or fuel containing environments (applied voltage ≥0.6 V) [11, 12].

The most common electrolyte material to date has been the stabilized zirconia with conductivity based on oxygen ions (O^{2-}), especially yttria-stabilized zirconia (Y_2O_3-

stabilized ZrO_2 or YSZ, $(ZrO_2)_{0.92}(Y_2O_3)_{0.08}$ for example) in which yttrium is added to the zirconia during manufacture. This choice is mainly due to performance and cost [5].

YSZ exhibits purely oxygen ionic conduction (with negligible electronic conduction). The crystalline array of ZrO_2 has two oxygen ions to every zirconium ion but in Y_2O_3 there are only 1.5 oxide ions to every yttrium ion. The dissolution of Y_2O_3 into ZrO_2 results in vacancies in the crystal structure where oxygen ions are missing. Oxygen ions from the cathode leap from vacancy to vacancy until they reach the anode. Basically, the yttrium oxide dopant serves dual roles: it stabilizes the high temperature cubic phase in zirconia and also generates oxygen vacancies [5, 24].

YSZ has good ionic conductivity at higher temperatures (>1000°C). For reduced temperature (700-850°C) operation, the lower oxygen ion conductivity (~0.8 eV) demands a very thin electrolyte layer [34]. It was earlier discussed that YSZ reacts with the cathode to form pyrochlore phases that are detrimental to cell performance. Yamamoto et. al. [36] have suggested that reaction between electrodes and electrolyte could be suppressed by inserting an interlayer of perovskite-type oxygen ion conductor such as $La_{0.9}Ba_{0.1}AlO_{2.95}$ and $Nd_{0.9}Sr_{0.1}AlO_{2.95}$.

2.3.4 Interconnect

The interconnect is a very critical component of SOFCs. Irrespective of planar or tubular cell configuration, the role of the interconnect is literally two-fold; it provides electrical connection between the anode of one individual cell to the cathode of neighboring one. It also acts as a physical barrier to protect the air electrode material from the reducing environment of the fuel on the fuel electrode side, and it equally

prevents the fuel electrode material from contacting the oxidizing atmosphere of the oxidant electrode side. The criteria for interconnect materials are the most stringent of all cell components. The most important requirements are chemical stability (high oxidation resistance), high electrical conductivity, thermal expansion coefficient close to that of an electrolyte material, high mechanical strength, gas tightness and machinability [1, 38]

Lanthanum chromite ($LaCrO_3$) is currently the most common candidate material since it exhibits adequate electronic conductivity in both fuel and oxidant atmospheres, moderate stability in both fuel cell environments as well as fairly good compatibility with other cell components in terms of phase, microstructure, and thermal expansion. The most daunting challenge for $LaCrO_3$ or doped $LaCrO_3$, up to now, is its extremely inferior sinterability in air due to easy volatilization of Cr (VI) species. Because of the volatilization, the predominant form of mass transport is a gaseous process mainly involving chromium oxide compounds. This leads to an evaporation/condensation mechanism of sintering in which the chromium ions evaporate in some form from the surface of the original grains and condense out onto the points of irregular contact, which are the areas of maximum surface energy. Because neck growth is accomplished without the transport of the material from the bulk of the grains, little densification or pore removal occurs. The poor sinterability of $LaCrO_3$ in air or oxidizing atmospheres is ascribed to the formation of a thin layer of Cr_2O_3 from CrO_3 gases at the interparticle neck during the initial stage of sintering [1, 39].

Besides $LaCrO_3$, some metal based interconnect materials are also promising. These are Fe based Cr alloys [39]. Brylewski et. al.[38] have observed that Fe-16Cr alloy

coated with $La_{0.6}Sr_{0.4}CoO_3$ reflects better conductivity and performance as compared to Sr doped $LaCrO_3$ in the same operating conditions.

CHAPTER 3

EXPERIMENTAL PROCEDURE

This section describes about the experimental techniques to fabricate alloy supported the SOFC with Co_2MnO_4 cathode. The alloy supported cells are more competitive in terms of mechanical properties and thermal shock resistance than traditional cermet supported cells. On the other hand, Co_2MnO_4 was tried as a new cathode material because of its good conductivity [55] and matching thermal expansion with other cell components. This spinel does not form any insulating or brittle compounds at the cathode electrolyte interface as is the case with conventional LSM cathodes.

3.1 Experimental Techniques Used

3.1.1 Tape Casting

Tape casting is also known as doctor blading and knife coating and under these names the process is well known in many industries, including paper, plastic, and paint manufacturing. In the ceramic industry, tape casting is most analogous to the traditional slip casting. The "doctor blade" is a scraper for the removal of excess substance to maintain a constant thickness of the coating [49].

In a typical tape casting process, the slip or slurry is poured into a puddle or reservoir behind the doctor blade, and the carrier to be cast upon is set in motion. The doctor blade gap between the blade and the carrier defines the wet thickness of the tape being cast. Other variables that come into play include reservoir depth, speed of carrier movement, viscosity of the slip, shape of the doctor blade, etc. The wet film of slip passes

into a drying chamber of some sort, and the solvents are evaporated from the surface, leaving a dry tape on the carrier surface. The tape casting process, equipment, and doctor blade with micrometer are shown in fig. 3.1 and 3.2.

Since tape casting is a "fluid forming" process, the choice and properties of solvent, dispersant, binder and plasticizer are of paramount importance. In the present work, toluene and ethanol were used as solvent. and Menhaden fish oil as dispersant. Polyvinyl butyral (PVB) was used as binder and butyl benzyl phthalate (BBP) as plasticizer.

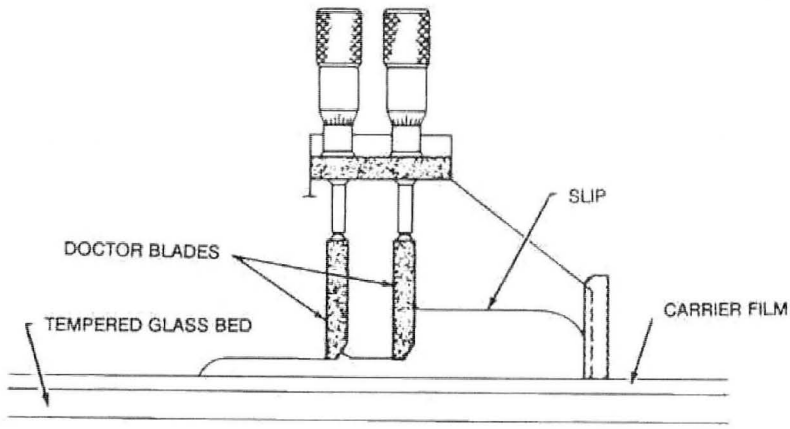

Figure 3.1(a) Tape casting process (schematic view)

Figure 3.1(b) Tape casting equipment

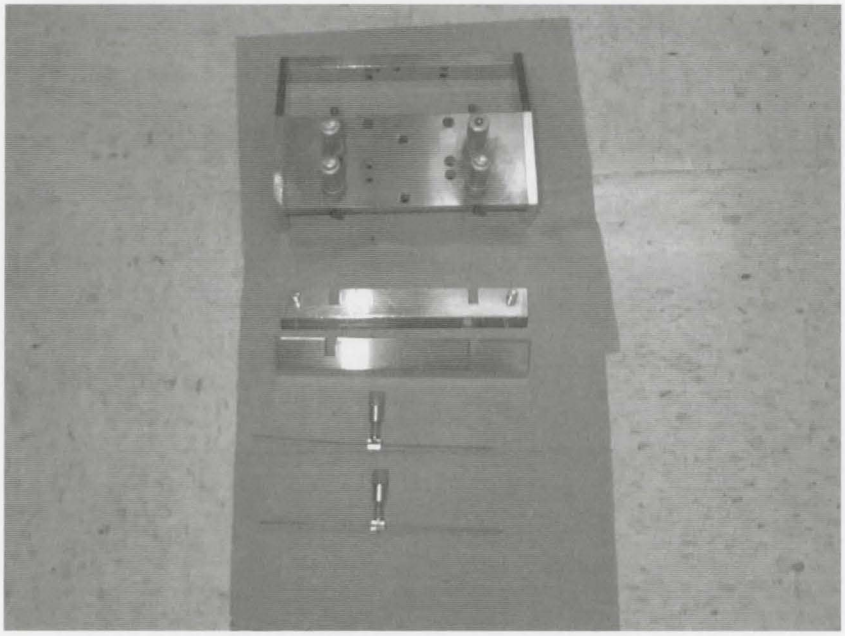

Figure 3.2(a) Doctor blades with micrometer (expanded view)

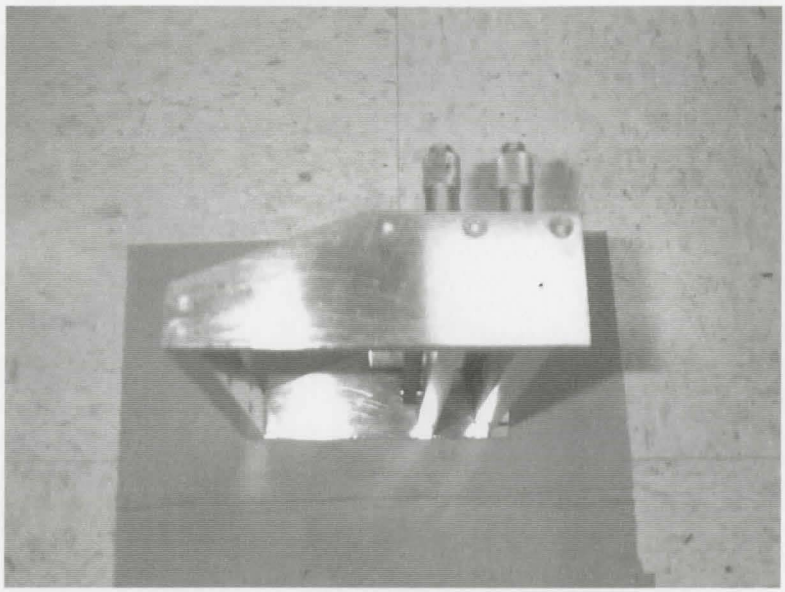

Figure 3.2(b) Doctor blades with micrometer (compacted view)

Fe_3O_4 and Cr_2O_3 powders were mixed in a 3:1 ratio of Fe: Cr. SEM micrographs of as-received powders of Fe_3O_4 and Cr_2O_3 are shown below.

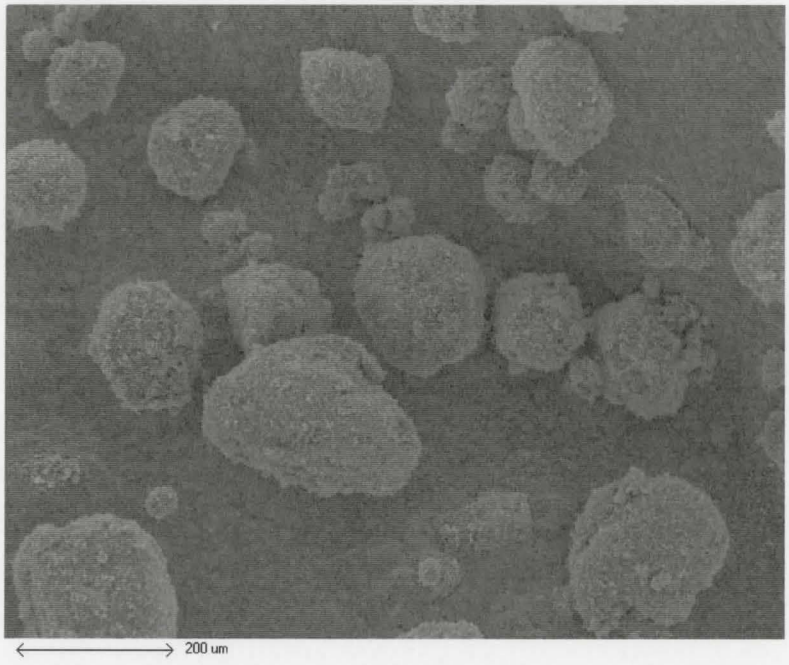

Figure 3.3 Fe_3O_4 powder particles

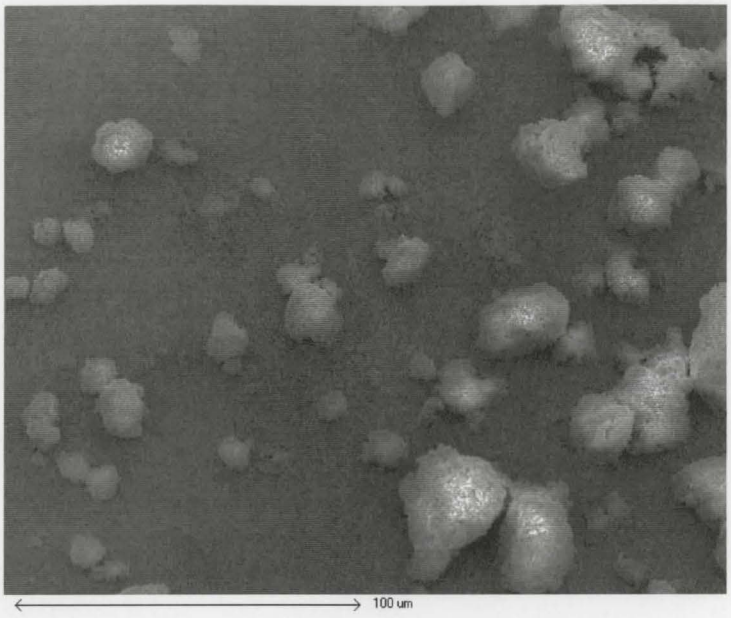

Figure 3.4 Cr_2O_3 powder particles

The powders were ball milled using zirconia balls for 6 h in ethanol medium. Milling was done in a small rotary mill at 35 rpm as shown in fig. 3.5.

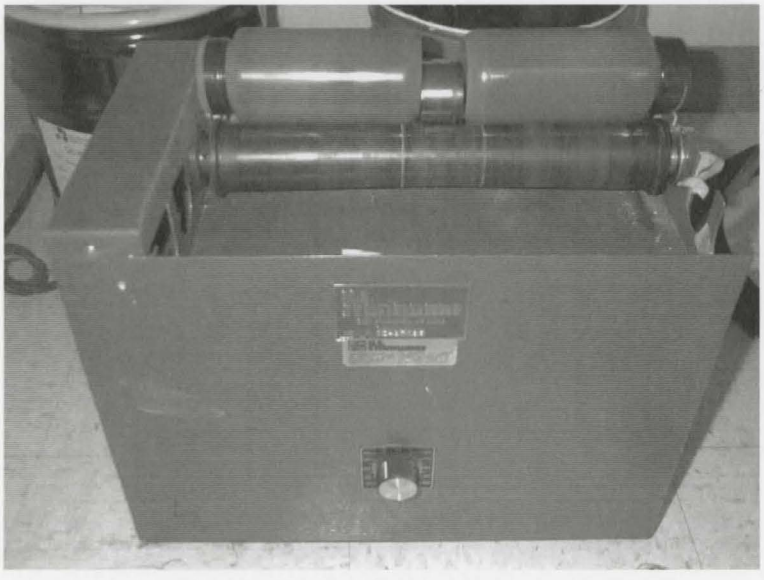

Figure 3.5 Milling machine for mixing

After the slurry was dried, a 20 g sample was put in a 125 ml Nalgene bottle with 30 zirconia balls. Approximately 30 volume percent of the bottle was filled with powder and balls. Fish oil, toluene, and ethanol were added to the bottle along with the powder mix. The bottle was then put on the ball mill. After 24 h of milling, the bottle was reopened and PVB and BBP were added along with graphite. The bottle was again sealed and put on the ball mill for 24 h. After the second stage of mixing, the slurry was ready for tape casting (fig.3.6). The composition of the slurry prepared is shown in table 3.1.

Components	**Amount (g)**
Fe_3O_4	15.077
Cr_2O_3	4.967
Fish oil	0.598
Toluene	8.585
Ethyl alcohol	7.385
Graphite	0.5
PVB (Poly vinyl butyral)	1.255
BBP (Butyl benzyl phthalate)	2.157

Table 3.1 Amount of various ingredients to prepare Fe_3O_4+Cr_2O_3 tape

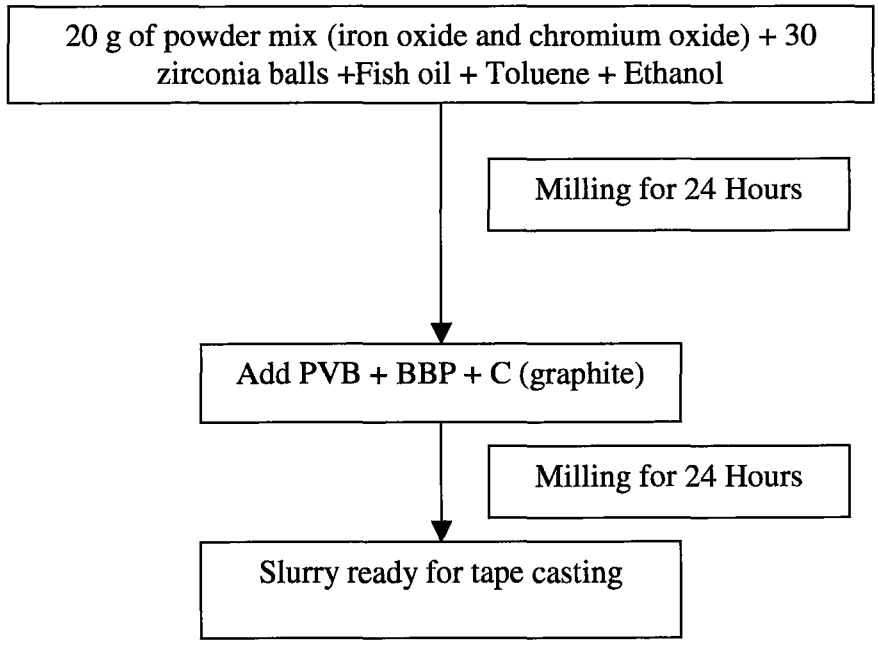

Figure 3.6 Powder slurry preparation steps for tape casting

3.1.2 Screen Printing

Screen printing is a process by which wet slurry could be deposited uniformly on a substrate. In the present case, the substrate was a green tape cast disc of iron oxide and chromium oxide. The substrate was placed on the screen printer (Fig. 3.7), held in position with the help of a vacuum pump and the slip was applied by use of a screen (Fig. 3.8) of appropriate size.

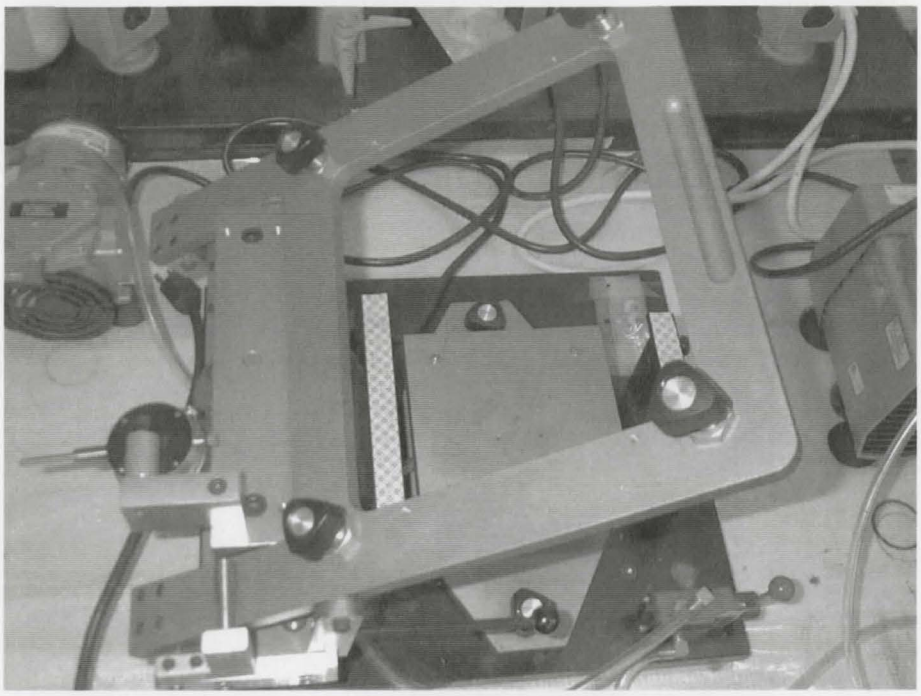

Figure 3.7 Screen printing equipment

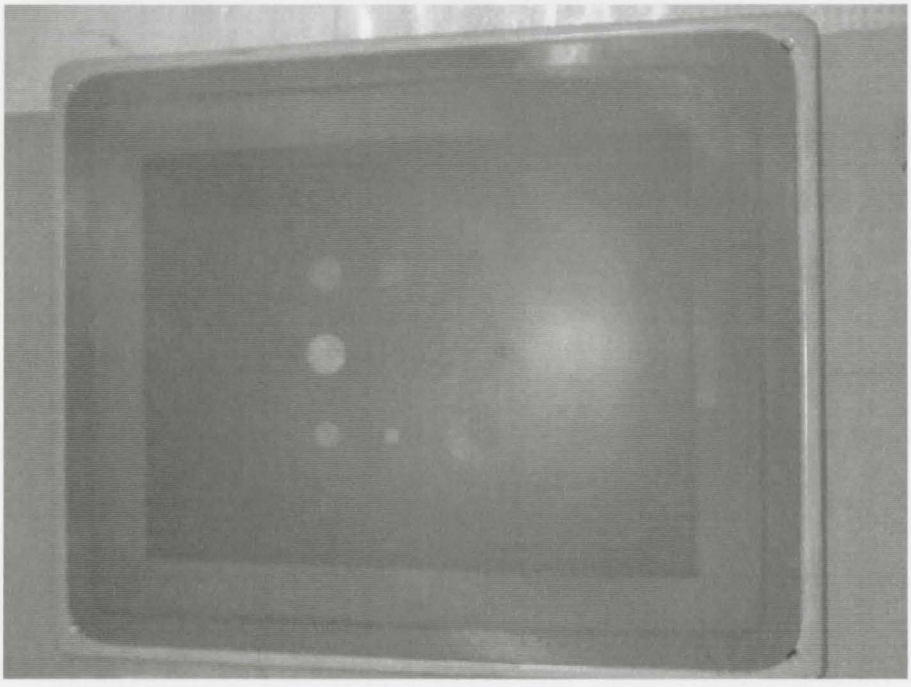

Figure 3.8 Single screen

As shown in fig. 3.8, the screen has pattern of various sizes. The rest is masked by a thin film of polymer. Screens are sensitive to contamination and must be cleaned after each use.

3.1.3 Dip Coating

Dip coating is a very elementary wet coating technique. A slurry of coating material is prepared and the sample is quickly dipped and extracted as film thickness varies with dipping time. Slurry viscosity and powder particle morphology are very important for good quality coating. The process from powder preparation to dip coating is depicted in fig. 3.9.

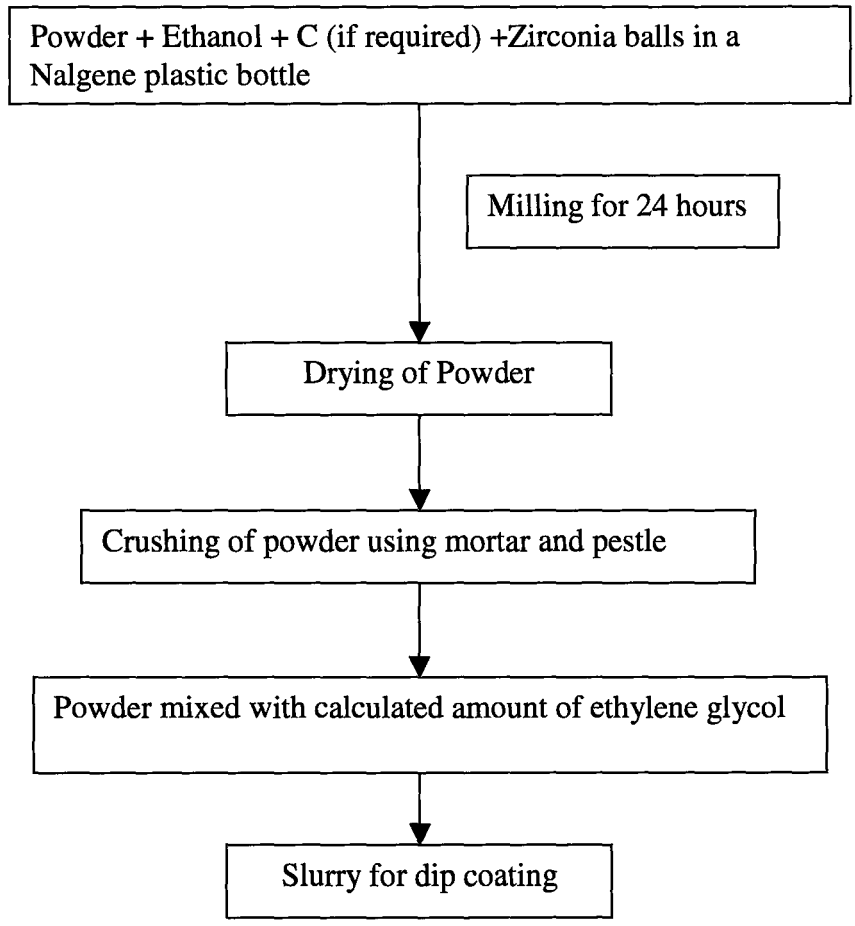

Figure 3.9 Flow chart for dip coating slurry preparation

3.2 Experimental Steps

3.2.1 Powder Preparation

It was the goal of the present work, to fabricate a metal supported SOFC having, Fe-Cr as the support, Ni/YSZ as anode, YSZ as electrolyte, and Co_2MnO_4 spinel as cathode. NiO (INCO F grade) (fig. 3.10) and YSZ (TOSOH) (fig. 3.11) were used as starting materials.

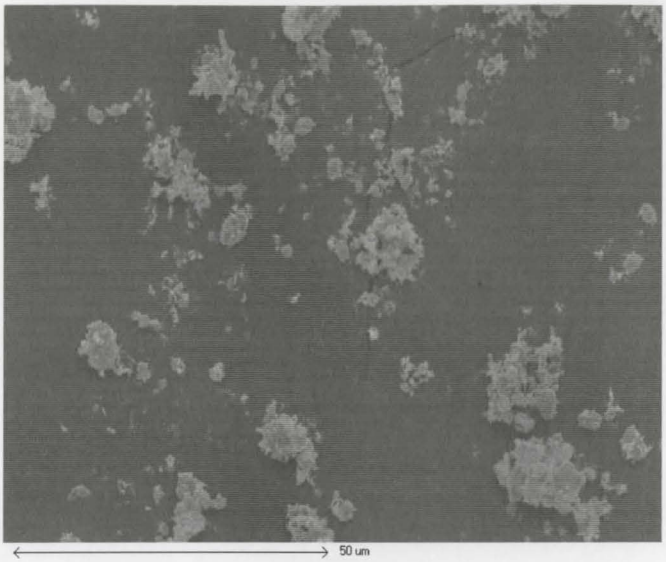

Figure 3.10 NiO powder particles

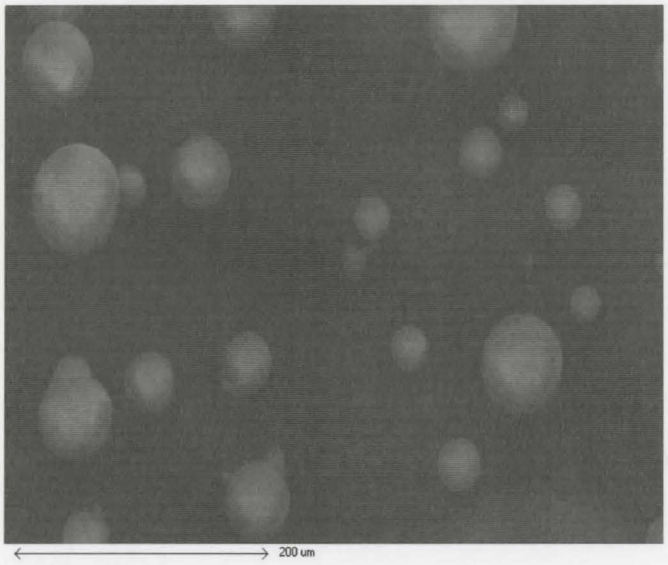

Figure 3.11 YSZ powder particles

For fabrication of the cathode (Co_2MnO_4), Co_3O_4 and MnO_2 were mixed in 2:1 proportions of Co: Mn and the powder mix was thermally treated according to shown cycle in fig.3.12.

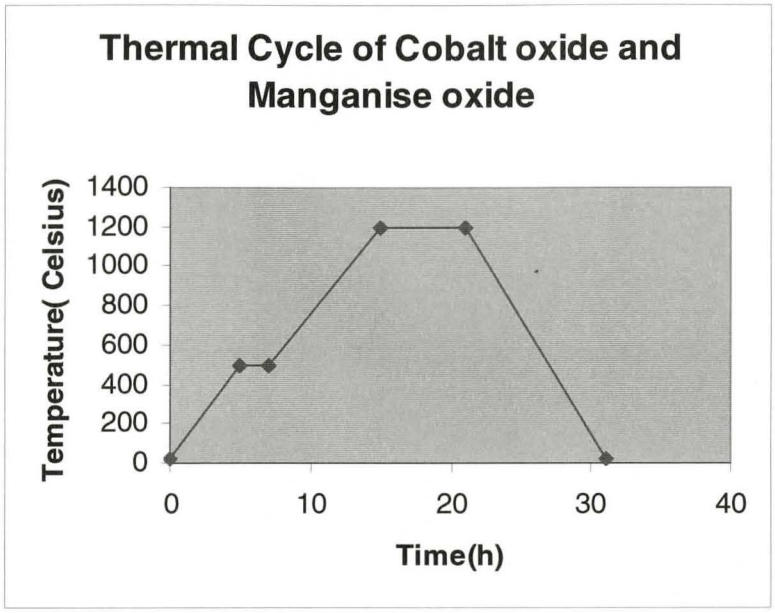

Figure 3.12 Co_2MnO_4 formation heat treatment

Co_2MnO_4 was expected to form according to phase diagram (fig.3.13) and governed by the following equation.

$2Co_3O_4 + 3MnO_2 = 3Co_2MnO_4 + 2O_2$

The XRD pattern (fig. 3.14) of the heat treated powder confirmed the formation of Co_2MnO_4.

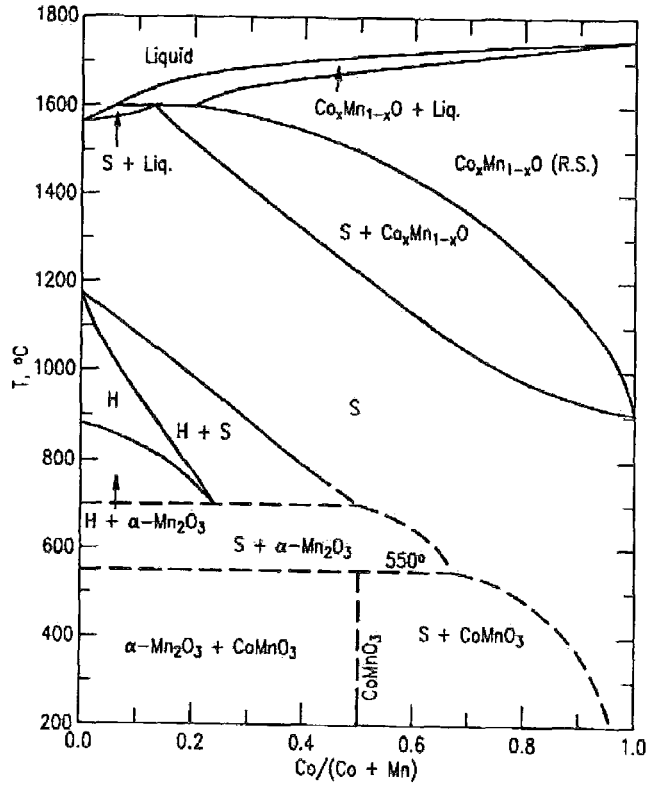

Figure 3.13 The Co-Mn oxide binary phase diagram [54]

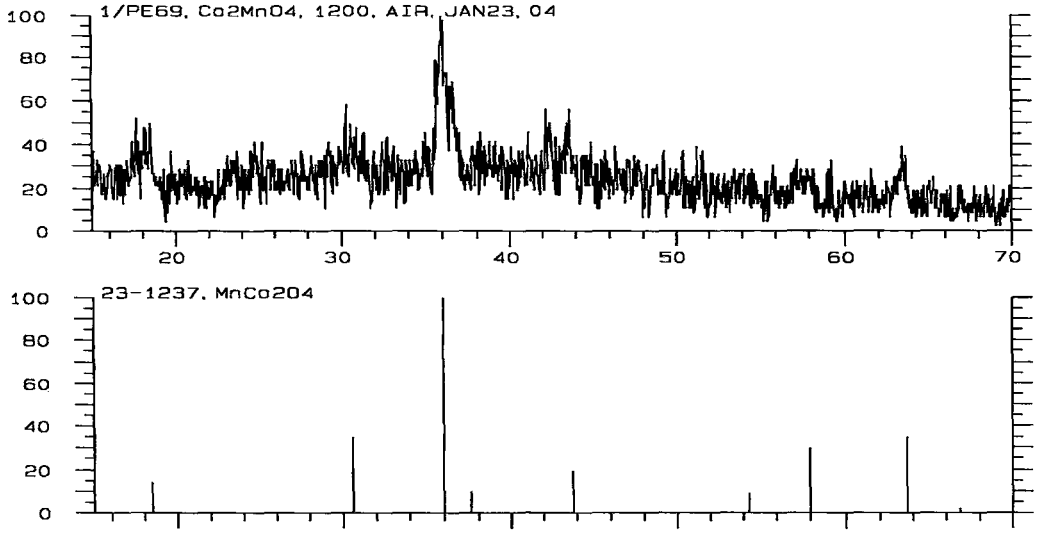

Figure 3.14 XRD pattern after heat treatment of Co_3O_4 and MnO_2 powders

3.2.2 Slurry Preparation for Screen Printing

The cathode (Co_2MnO_4) was screen printed on the electrolyte during fabrication of the cell. Co_2MnO_4 powder was thoroughly mixed along with various chemicals (Table 3.2) in a mortar and pestle to yield good quality slurry (paste).

Constituents	Amount
Powder	4.549 g
Paste preparation chemical(OS 430)	5.05 g
Graphite	0.609 g
Terpine oil	2 ml

Table 3.2 Co_2MnO_4 slurry composition for screen printing

3.2.3 Slurry Preparation for Dip Coating

The anode and electrolyte were fabricated by using the dip coating process (fig.3.9). The amount of various constituents to prepare the slurry for anode and electrolyte are given in tables 3.3 and 3.4 respectively.

Constituents	Amount
NiO	3 g
YSZ	10 g
Fe_3O_4	5.1 g
Cr_2O_3	1.9 g
C(4023)	4 g

Table 3.3 (a) Powder mix composition for anode dip coating slurry

Constituents	Amount
Powder mix	5.00 g
Ethylene glycol	25.329 g

Table 3.3 (b) Slurry composition for anode dip coating

Constituents	Amount
YSZ	5 g
Ethylene glycol	20.032 g

Table 3.4 Slurry composition for electrolyte dip coating

3.2.4 Tape Casting

Tapes of support material (Fe_3O_4 + Cr_2O_3), having wet thickness of 300 micron and composition as listed in table 3.5, were cast and punched into discs of 25 mm diameter (fig. 3.15). Punched discs were stacked together, pressed with a load of 1.5 tonne and subjected to the heat treatment shown in (fig.3.16).

Constituents	Amount (gm.)
Fe_3O_4	15.077
Cr_2O_3	4.967
Fish oil	0.598
Ethyl alcohol	7.385
Toluene	8.585
PVB	1.255
BBP	2.157
Graphite	1.034

Table 3.5 Amount of various constituents in support tape casting slurry

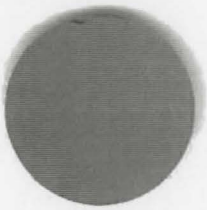

Figure 3.15 Punched disc of stacked tapes of support material

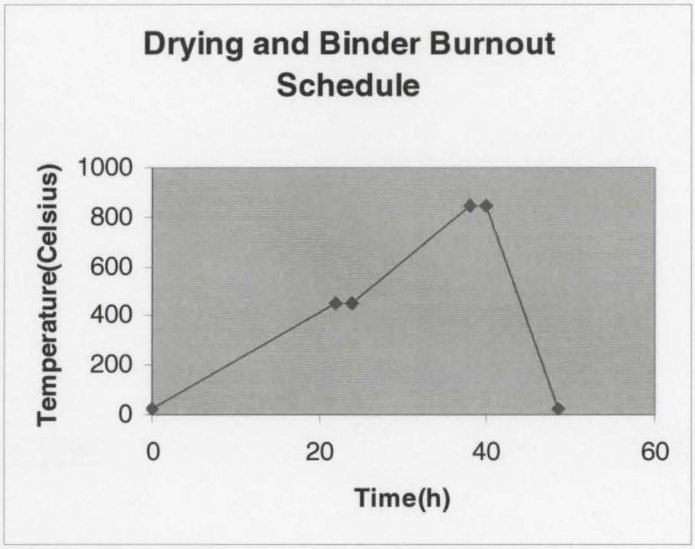

Figure 3.16 Binder burnout schedule for metal oxide support

3.2.5 Dip Coating and Drying (Binder Burnout)

After the binder burnout treatment, the support was first dip coated with NiO + YSZ + Fe_3O_4 + Cr_2O_3 + C anode slurry and dried. The dip coating process was repeated with YSZ electrolyte slurry followed by drying. Dip coated layers was dried according to following thermal cycle (fig. 3.17).

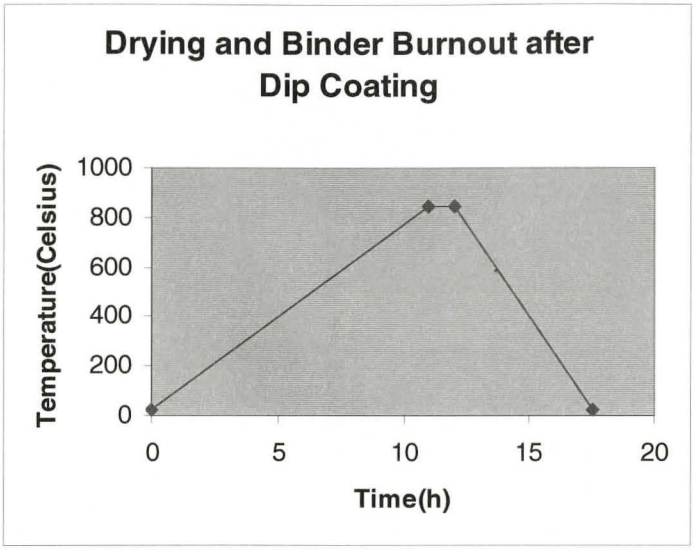

Figure 3.17 Drying and binder burnout cycle after each dip coating

3.2.6 Co-firing

After YSZ dip coating, the cell was sintered at 1350°C for 10 h. Heating and cooling rates are very important for co-sintering of various layers without delamination (fig. 3.19). Various samples were tested for the optimum heating and cooling rate in this process; dilatometry results (fig. 3.18) for various cell components at the working temperature range were very useful. Figure 3.2.6.1 suggests that in the temperature range between 800°C to 1200°C, different cell layers have different shrinkage patterns which cause delamination, so heating rate should be kept high enough for all the layers to be co-sintered without allowing layers enough time to be delaminated. Therefore, a heating rate of 400°C/h and a cooling rate of (150°C/h) was sufficiently low to accommodate thermal stresses.

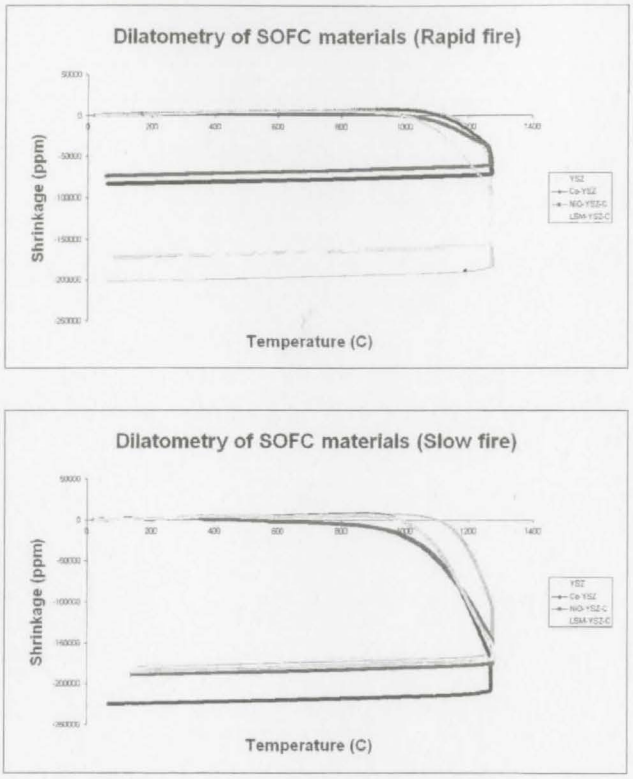

Figure 3.18 Dilatometry results of YSZ and NiO/YSZ [50]

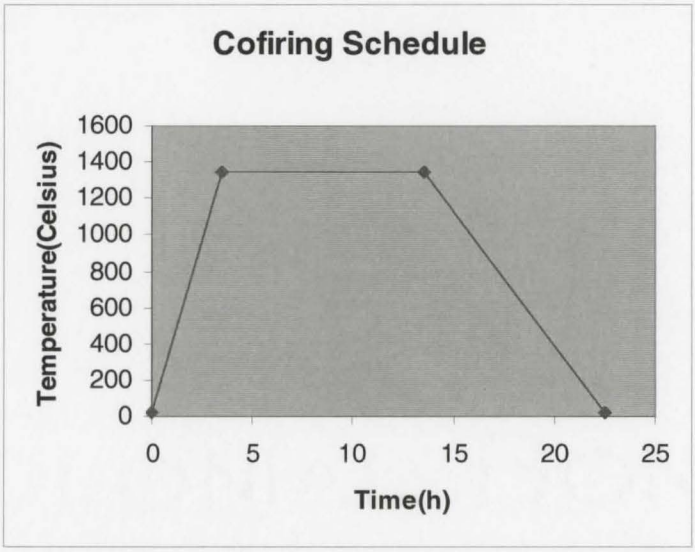

Figure 3.19 Co-firing thermal schedule for support, anode, and electrolyte

3.2.7 Cathode screen printing and sintering

The cathode (Co_2MnO_4 paste) was screen printed on the co-fired sample. After one time screen printing, the thickness of the wet coating was approximately 90 microns. Now, the complete cell was put into the furnace for cathode binder burnout and subsequent sintering (fig. 3.20). The complete cell prior to reduction is shown in fig. 3.21. It has a 0.9 cm. cathode (Co_2MnO_4) diameter screen printed on the YSZ electrolyte layer and has an active area of 0.636 cm^2. The diameter of the cell is 19 mm reflecting 25% shrinkage during sintering.

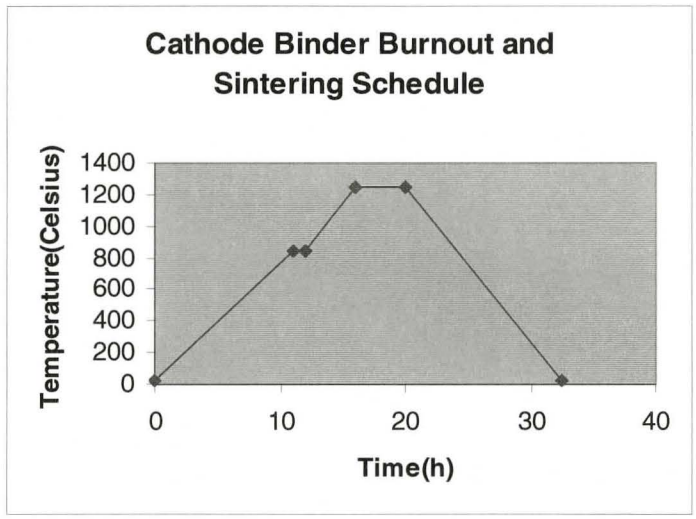

Figure 3.20 Thermal cycle for screen printed cathode

Figure 3.21 Complete cell after sintering

3.2.8 Final Reduction

The fully fired cell was put into a furnace and reduced in a hydrogen atmosphere. The reduction process also introduced porosity because of loss of oxygen.

The cell was slowly heated to 950°C in air, then Ar was passed for 20 minutes followed by ultra high purity hydrogen for 10 h and finally cooled to room temperature. This sequence was necessary to inhibit cracking of the interlayer because of non-uniform thermal expansion/contraction.

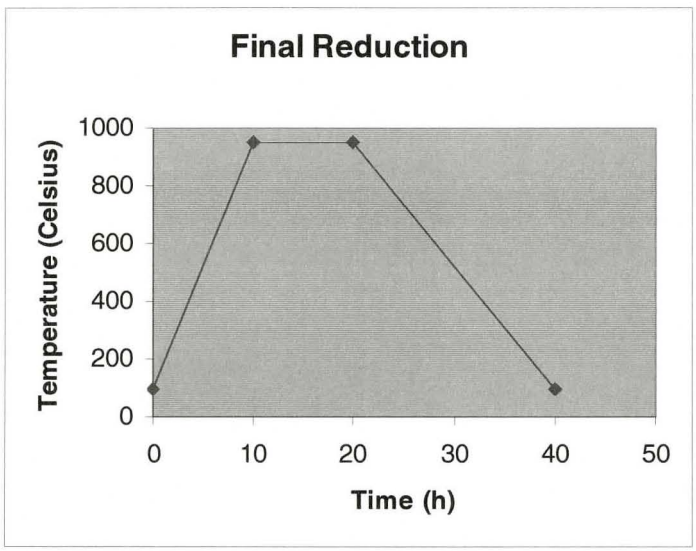

Figure 3.22 Reduction schedule of cell prior to testing

3.2.9 Summary

The complete experimental procedure is shown in the following flow chart (fig.3.23)

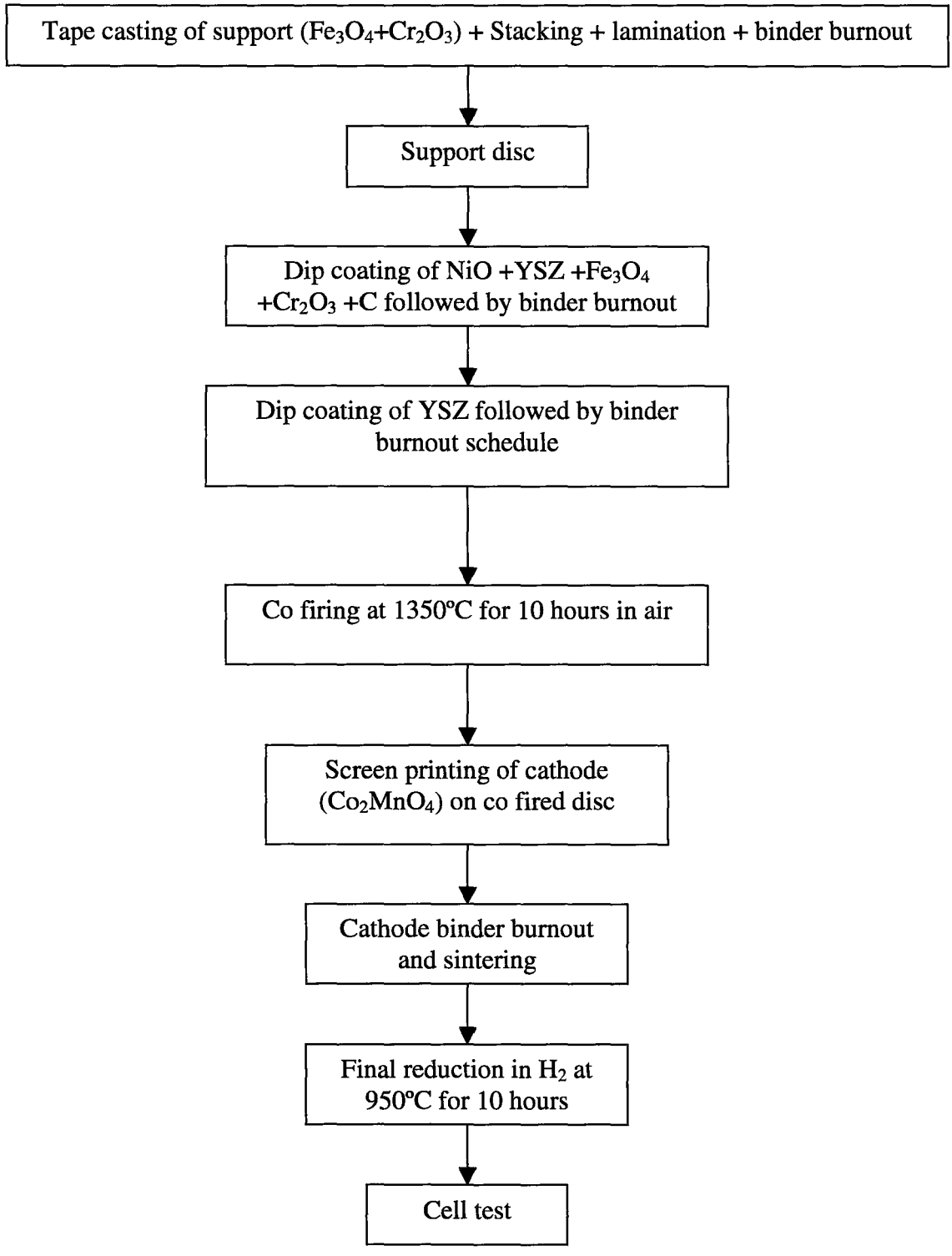

Figure 3.23 Complete Experimental procedure

CHAPTER 4

RESULTS AND DISCUSSION

4.1 Fabrication of the Support (Substrate)

4.1.1 Green Pellet

Commercially available powders of Fe_3O_4 and Cr_2O_3 were mixed in a 3:1 Fe:Cr proportion with solvent, dispersant, binder and plasticizer for tape casting. Discs of 25 mm diameter and 300 micron thickness were cut and stacked together and pressed in a die to form the support layer. These discs were slowly heated in the furnace to 850°C for binder burnout. After binder burnout the discs had sufficient strength and porosity for dip coating. An SEM photo of the disc cross-section is shown in fig. 4.1.

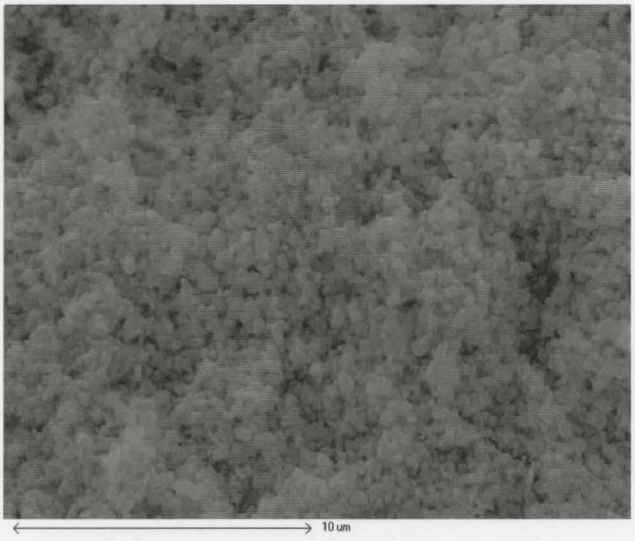

Figure 4.1 Arrangement of particles after binder burnout at 850°C

This figure reveals homogeneous particle stacking and a narrow distribution of Fe_2O_3 and Cr_2O_3 particle sizes. These nearly monosize particles are obtained by ball milling of the slurry for 48 h to be used for tape casting.

4.1.2 Sintering of Pellets

When these discs were sintered at 1350°C for 10 h they exhibited up to 25% shrinkage and increased strength. The SEM photo of the cross-section (fig. 4.2) shows densification with some particle ripening (grain growth).

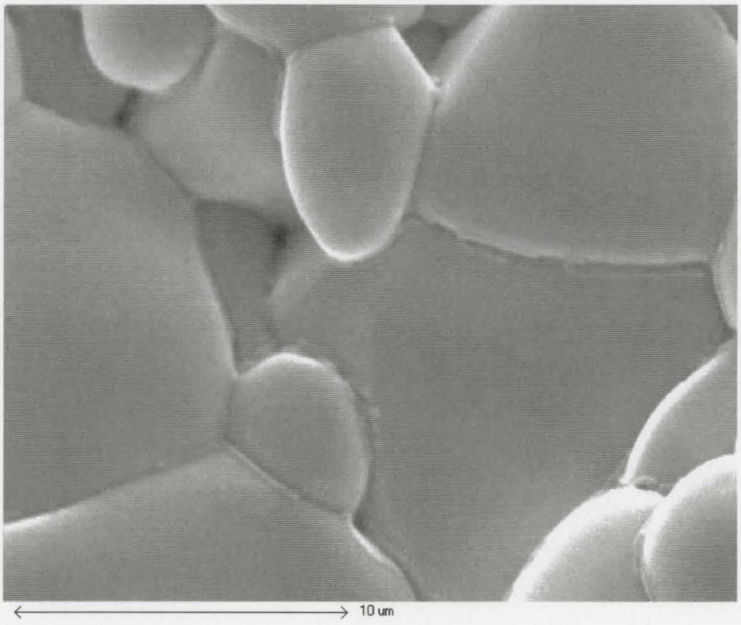

Figure 4.2 SEM of cross section of sintered support

XRD of the sintered pellet revealed the formation of the corundum phase $(Fe-Cr)_2O_3$ (fig. 4.3). This is also supported by phase equilibria (fig. 4.4) calculated for this system by using Fact Sage software.

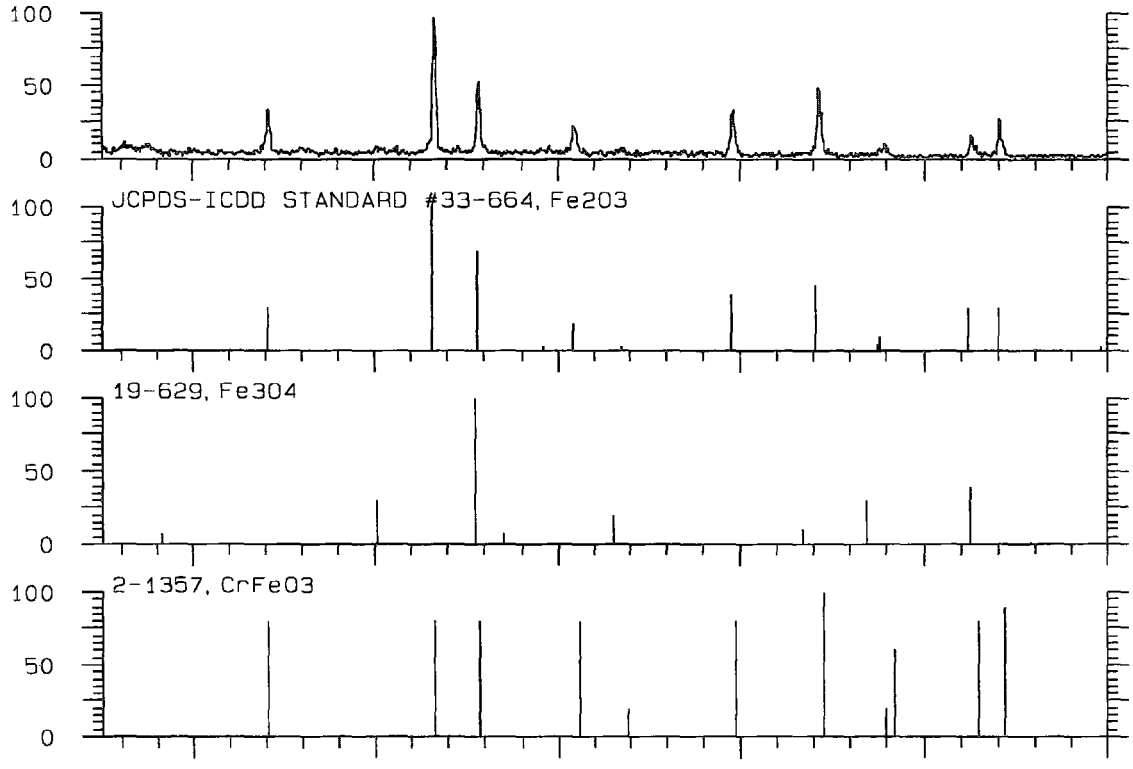

Figure 4.3 XRD pattern of support at 1350°C

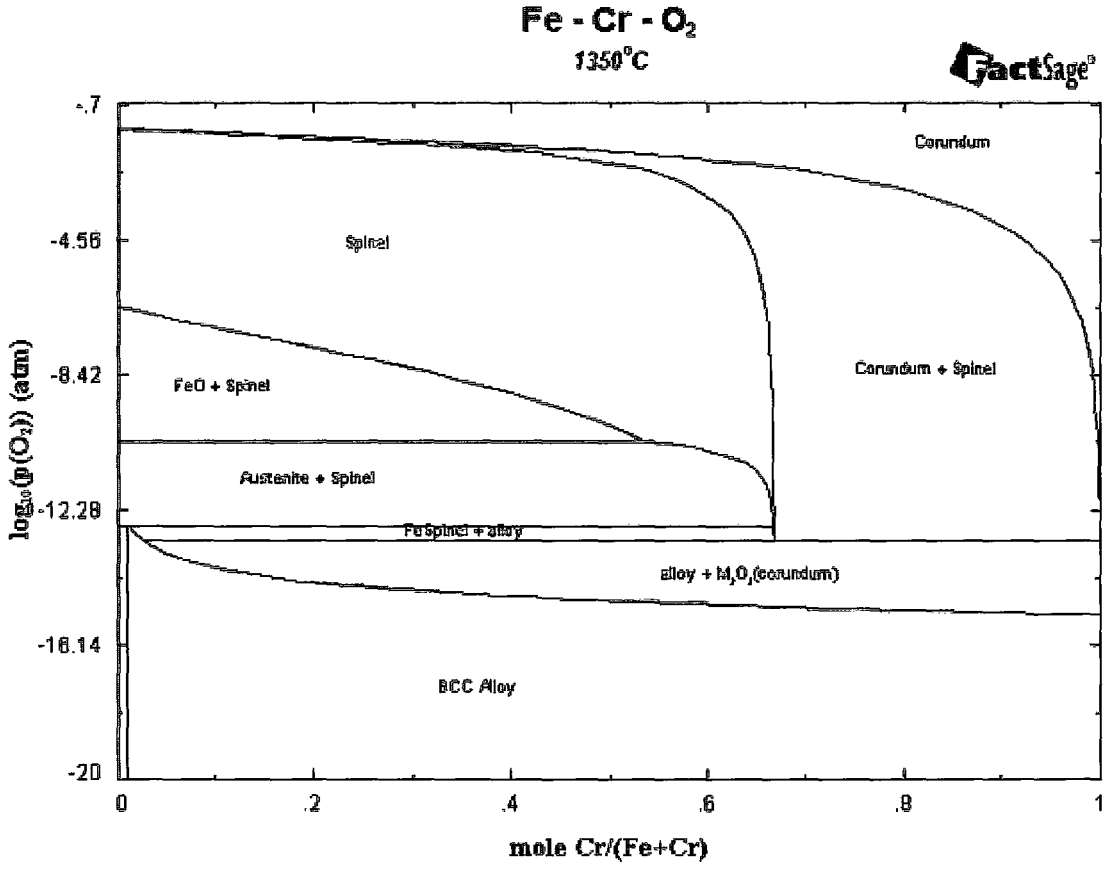

Figure 4.4 Various Phases of Fe-Cr-O_2 at 1350°C

4.1.3 Reduction of Support after Sintering

By observing Ellingham diagram (fig. 4.5) for the reduction of support, it can be seen that among NiO, Cr_2O_3, and FeO, Cr_2O_3 is the most difficult to reduce. Thermodynamically, it can not be reduced below 800°C until $P(H_2O)/P(H_2)$ is 10^{-5}. Water is the byproduct of the reduction reaction and therefore $P(H_2O)$ will increase causing reduction equilibria to shift in such a way so as to stop the reaction. Reduction is

maintained by using ultra high purity hydrogen gas that contains approximately 2 ppm water vapor as impurity and a continuously flowing stream.

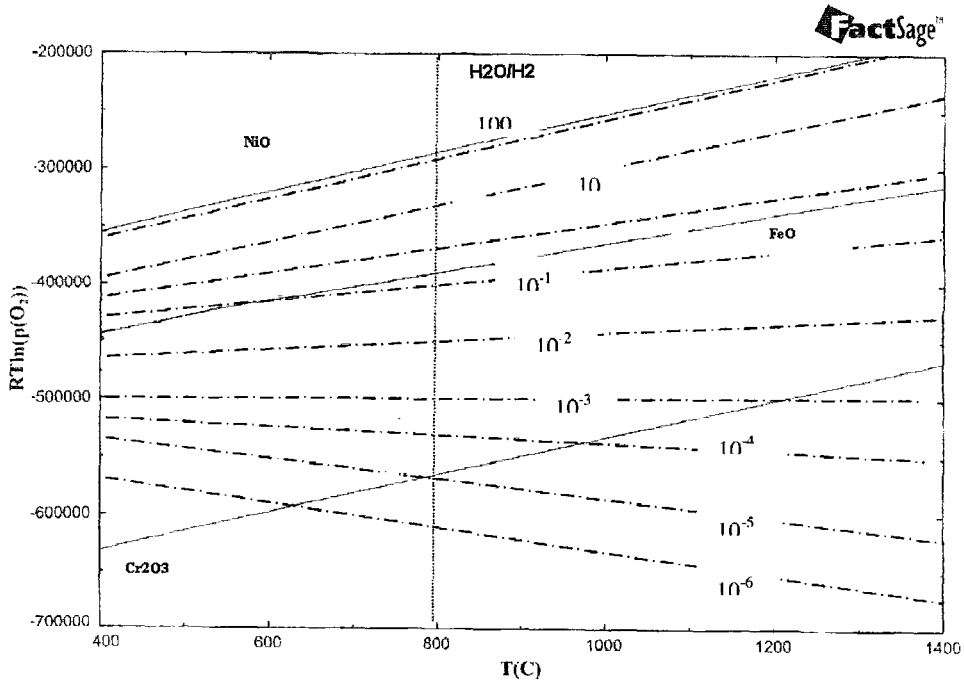

Figure 4.5 Ellingham diagram of Ni, Fe, and Cr with H_2/H_2O ratios superimposed

An approximate phase stability diagram (fig.4.5), generated by Fact Sage software, reflects the stability range of Fe and Cr above 700°C. Taking these points into the consideration, four samples were prepared and after sintering they were subjected to reduction at 900°C, 950°C, 1050°C, and 1150°C for 10 hours each in hydrogen atmosphere. The XRD patterns of reduced samples are shown in fig. 4.7(a, b).

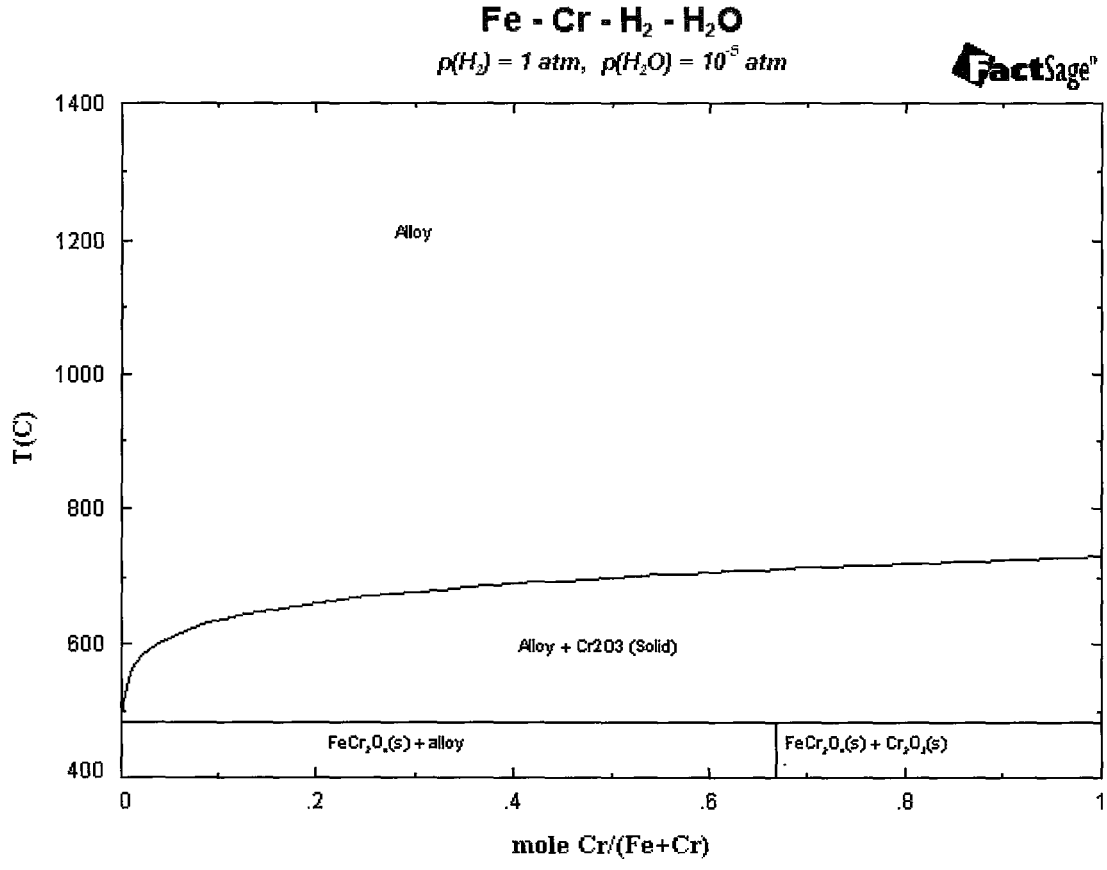

Figure 4.6 Phase stability in Fe-Cr-H_2-H_2O system for hydrogen containing 10 ppm H_2O

XRD analysis showed Fe and Cr as prominent phases along with $FeCr_2O_4$, and Cr_2O_3 as minor phases. The amount of the minor phases further decreased from 900°C to 1150°C. This deviation from the phase diagram prediction is possibly due to kinetic factors. As we can see at 1150°C, the support pellet was composed of almost single phase of pure Fe and Cr. Therefore this temperature could be considered as temperature for almost full conversion of corundum phase into the respective metals in the given experimental conditions.

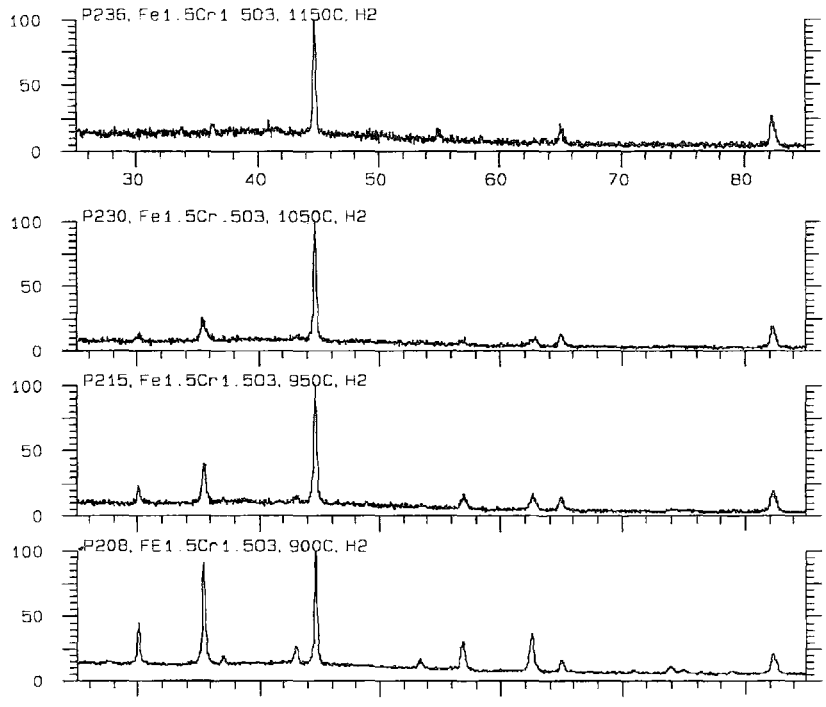

Figure 4.7 (a) XRD patterns after reduction of support at 1150°C, 1050°C, 950°C, and 900°C

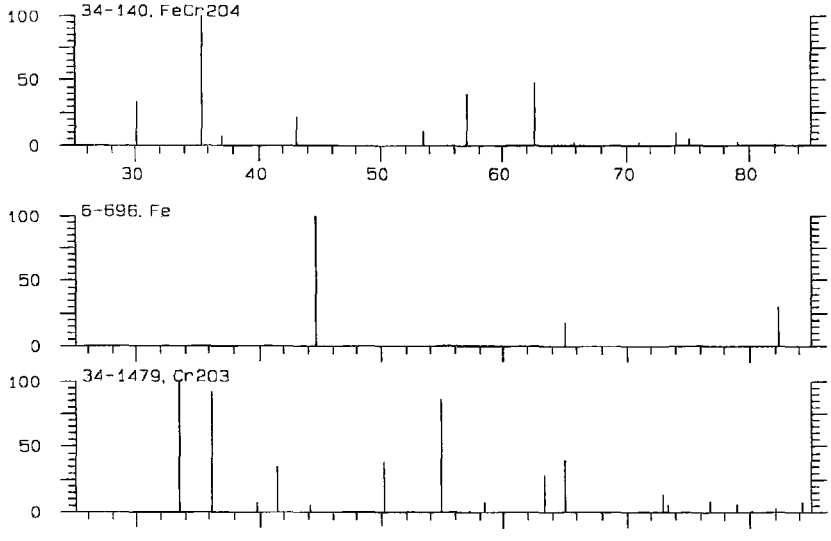

Figure 4.7 (b) JCPDS XRD patterns of $FeCr_2O_4$, Fe, and Cr2O3

It was observed that after reduction at 1050°C and at 1150°C, the pellet was shattered. This behavior can be attributed to the fact that during reduction, the material undergoes loss of oxygen and this loss of oxygen causes inhomogeneous stress generation in the pellet. These stresses are responsible for fracture of the pellet during reduction. To solve this problem, the reduction temperature was lowered which decreased the rate and extent of reduction and allowed sufficient stress relief to prevent cracking. At 950°C the pellet contained approximately 80% alloy (Fe and Cr) and 20% oxides. Reduction also helped to introduce porosity in the support to enable gas flow during cell testing as can be seen in the SEM micrograph (fig. 4.8) of the reduced support disc.

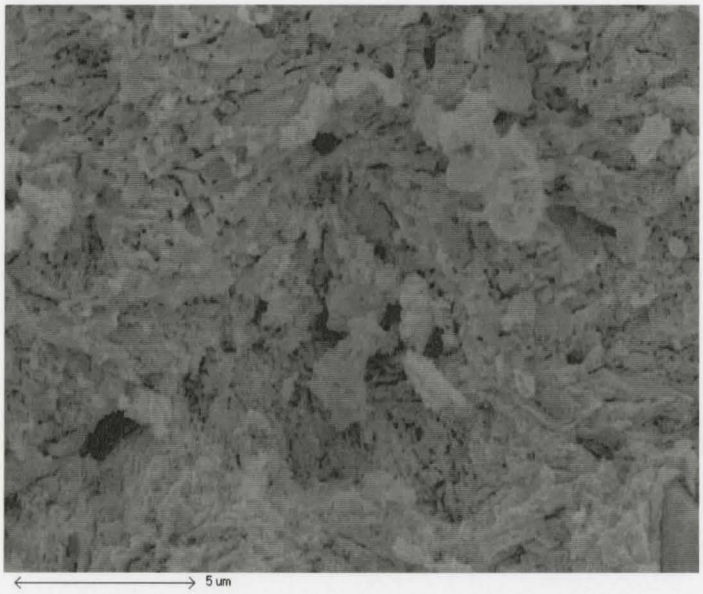

Figure 4.8 SEM pattern of the sintered support after reduction at 950°C for 10 h

4.2 Observations with Co_2MnO_4 (Cathode)

In the present study Co_2MnO_4 was tested as a candidate for a cathode material in conjunction with the metal support. Since the cathode was to be screen printed after complete firing of all other layers and then sintered, and reduced during the cell fabrication process, it was necessary for the cathode to reoxidize to spinel form during cell testing. Therefore it is essential to assess the phase and mechanical stability of Co_2MnO_4 in reducing and oxidizing conditions. To check this, pellets of Co_2MnO_4 were prepared. A micrograph of the cross-section of a green pellet is shown in fig. 4.9.

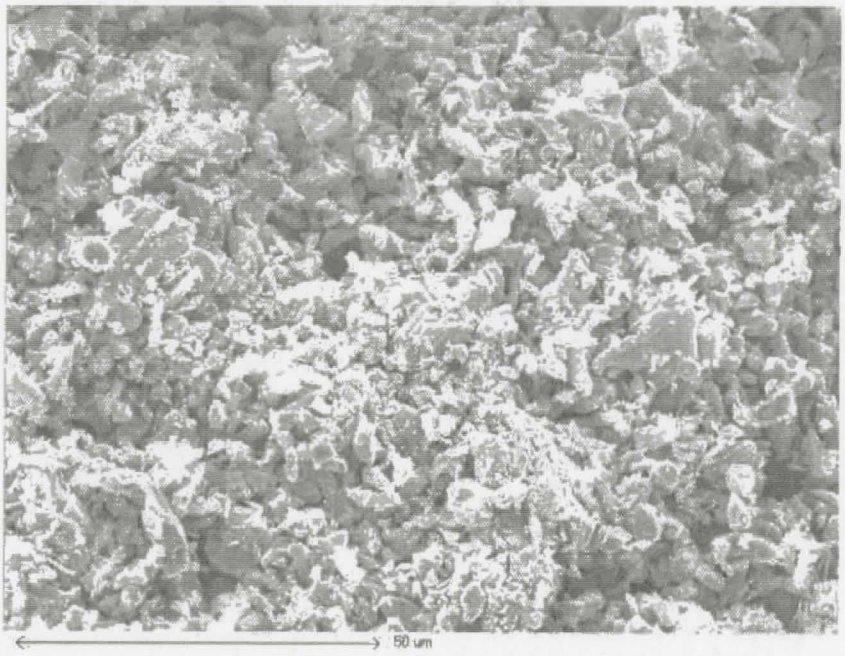

Figure 4.9 SEM micrograph of pressed green pellet of Co_2MnO_4

4.2.1 Sintering and Reduction of Pellet

Green pellets were sintered at 1250°C in air and subsequently reduced in forming gas (7% H_2, 93%N_2) at 900°C for 4 h. The sintering temperature was chosen to avoid melting the pellet (fig. 4.10).

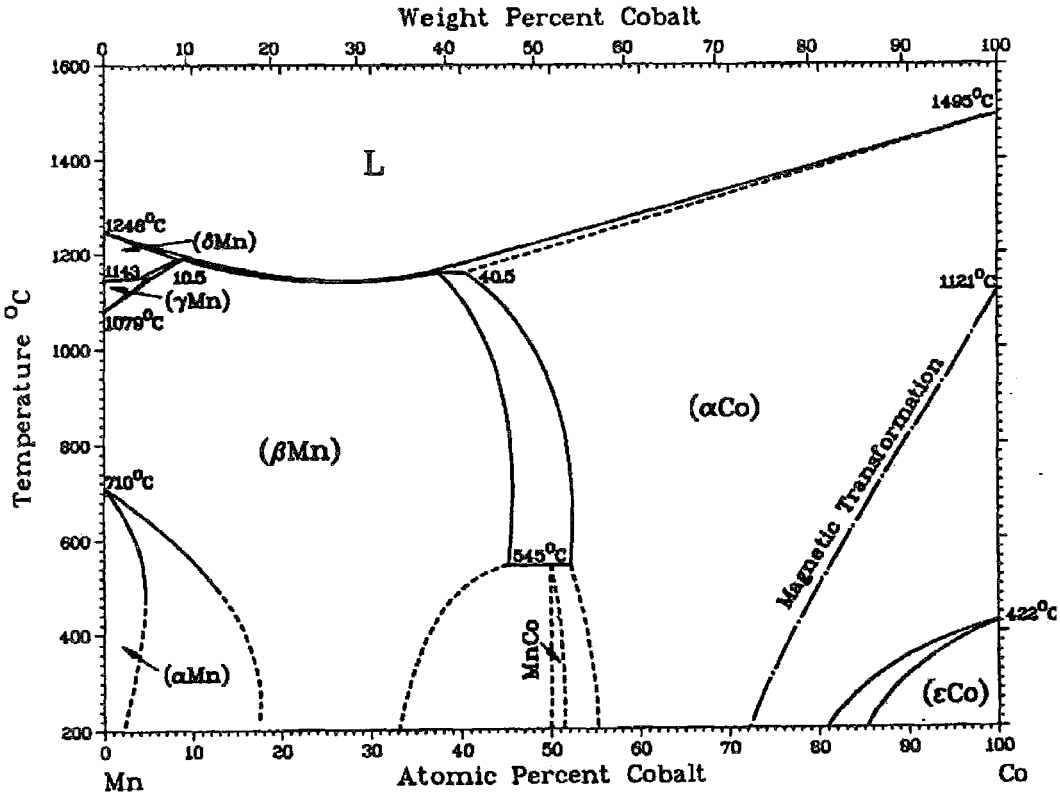

Figure 4.10 Co-Mn Phase diagram [57]

The XRD pattern (fig. 4.11) revealed that the pellets were easily reduced into MnO and different crystallographic forms of Co. The SEM micrograph (fig. 4.12) shows a porous structure due to reduction along with streaks that reflects the possibility of partial melting.

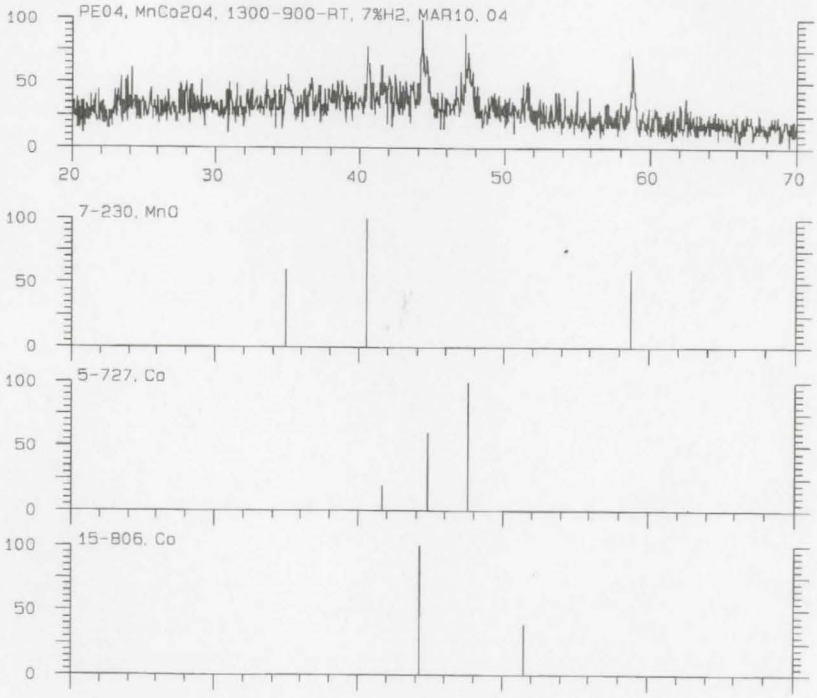

Figure 4.11 XRD pattern of reduced Co_2MnO_4

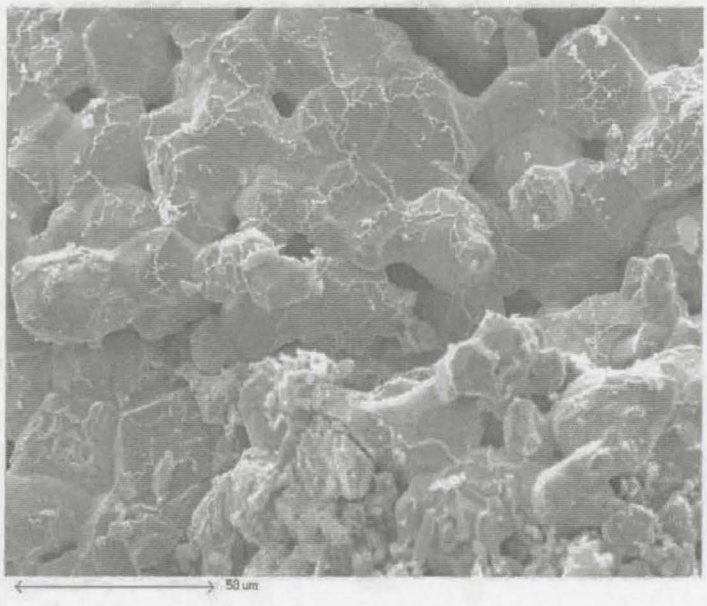

Figure 4.12 SEM micrograph of Co_2MnO_4 reduced at 900°C for 4 h

4.2.2 Phase Recovery during Re-Oxidation

The reduced Co_2MnO_4 pellet was oxidized in air at 800°C. The XRD pattern (fig. 4.13) after 6 hours oxidation shows the formation of Co_2MnO_4 along with Co_3O_4.

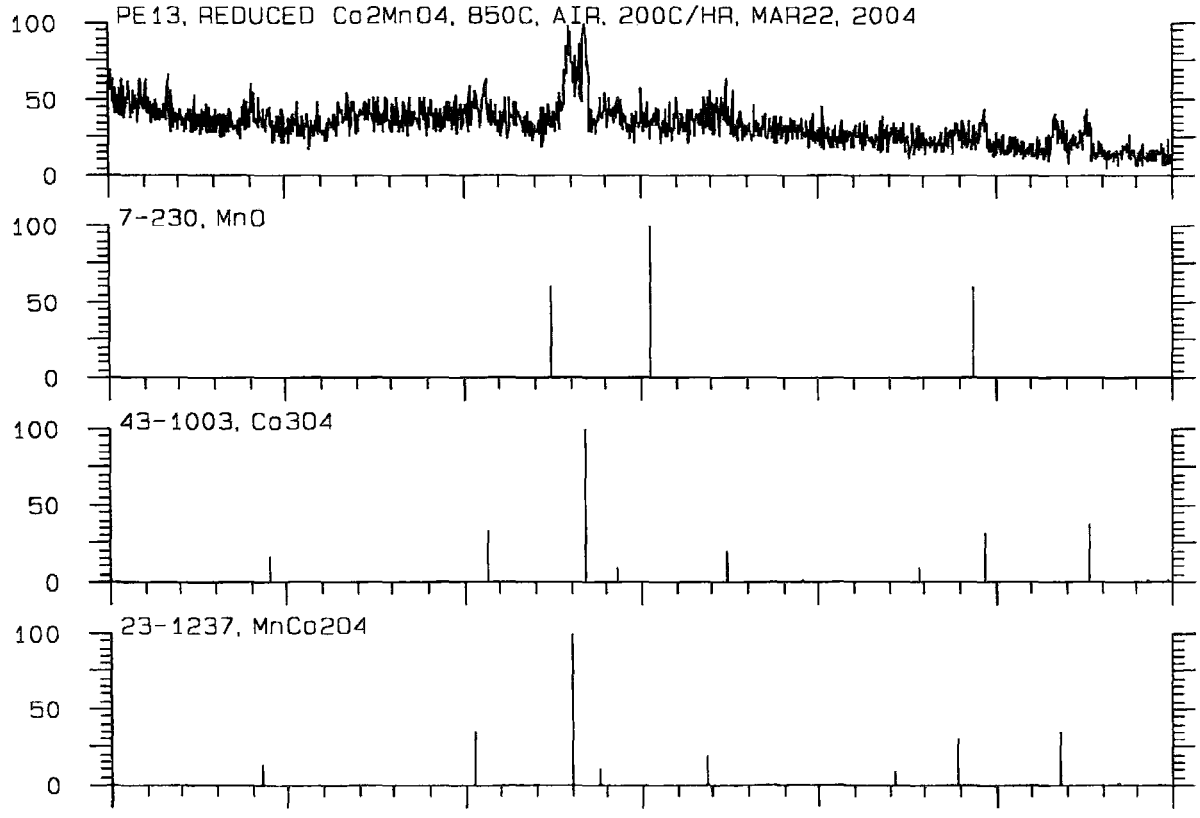

Figure 4.13 XRD pattern after 6 hours oxidation of MnO + Co pellet

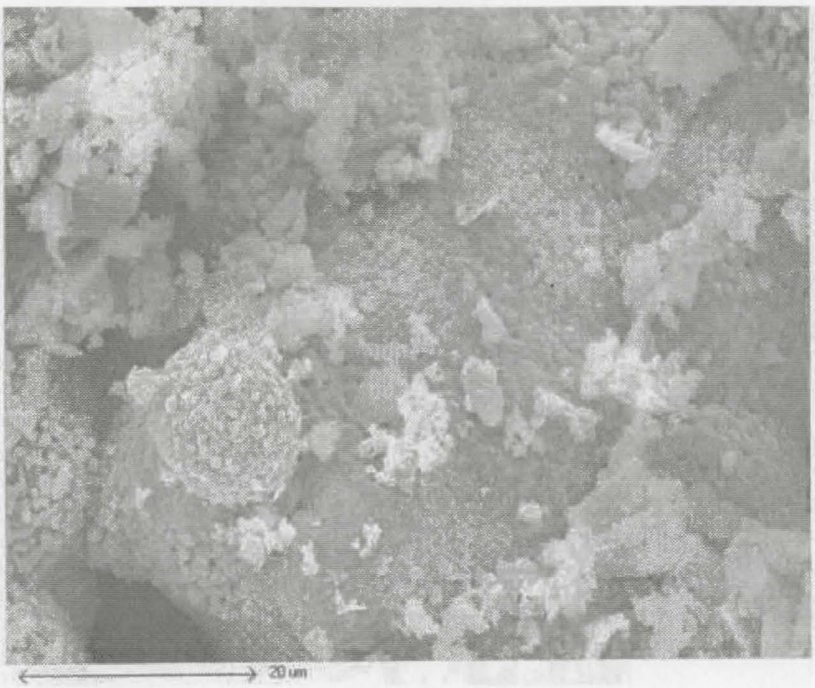

Figure 4.14 SEM micrograph of MnO + Co pellet after 6 hours oxidation

The SEM micrograph (fig. 4.14) of the sample after 6 hours oxidation revealed agglomerated nodules without any streaks as in fig. 4.12. There is also a decrease in porosity of the pellet. The pellet was then oxidized for 45 hours to assess the kinetics of the recovery of the Co_2MnO_4 phase. XRD analysis (fig. 4.15) showed approximately 80% Co_2MnO_4 was recovered and remaining phases were Mn_2CoO_4 and Co_3O_4. This shows that the recovery of spinel phase occurs at a slow rate. Examination by SEM (fig. 4.16) revealed more fine pores but a decrease of total porosity.

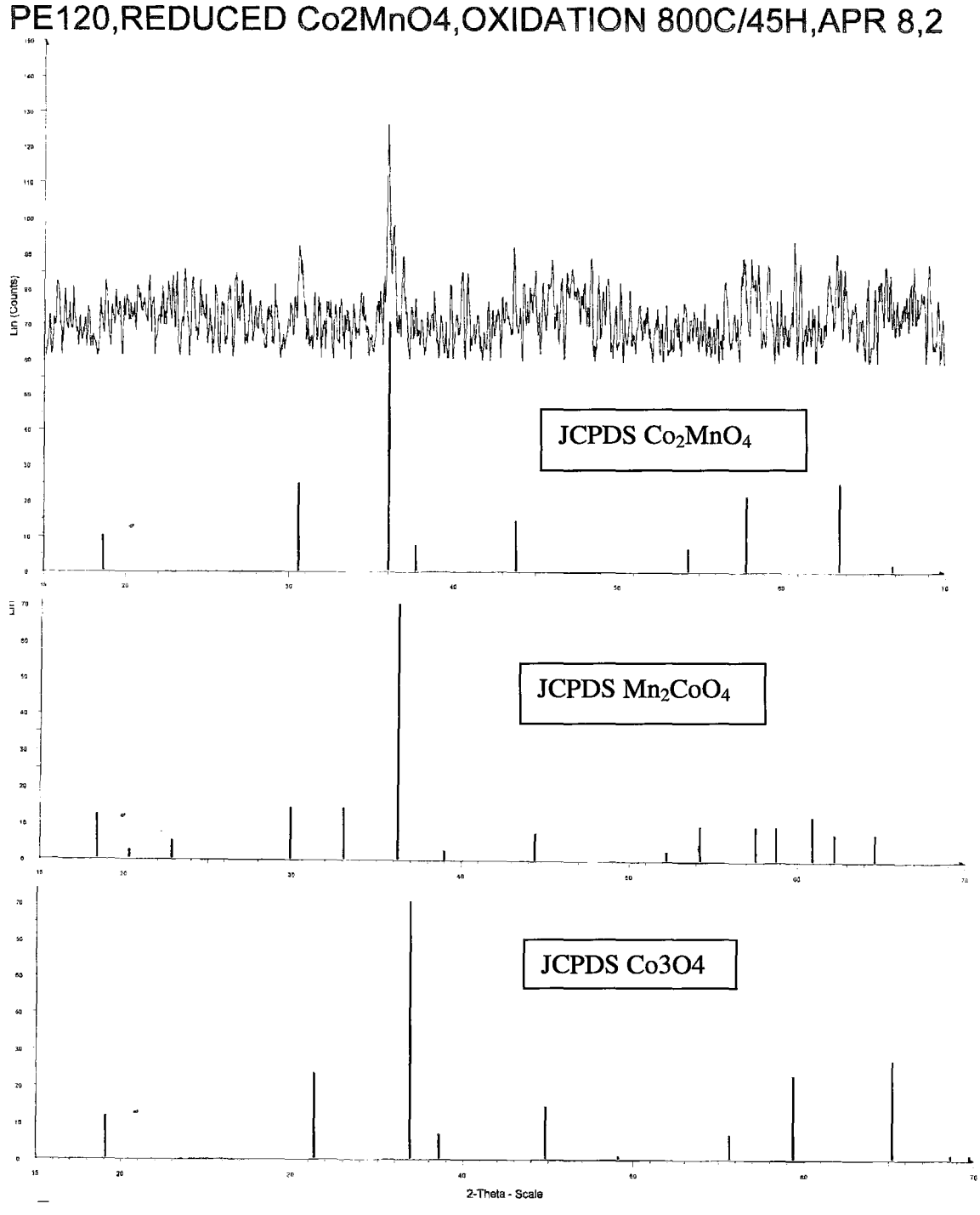

Figure 4.15 XRD pattern of Co_2MnO_4 reduced to Co + MnO and re-oxidized for 45 h at 800°C

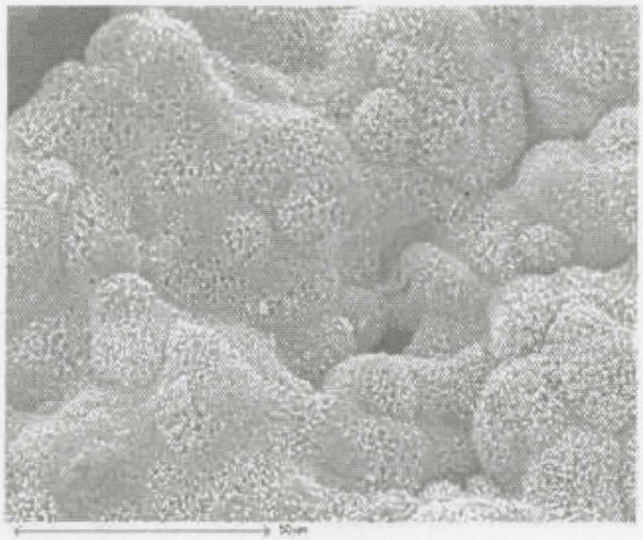

Figure 4.16 SEM micrograph of Co_2MnO_4 after reduction and 45 hours oxidation at 800°C

4.3 Observations with Complete Cell

The anode and electrolyte were dip coated onto the support and co-fired at 1350°C for 10 hours. The cathode was then screen printed on the electrolyte and the complete cell was sintered at 1250°C for 4 h. An SEM micrograph of the complete cell is shown in fig. 4.17.

The boundary between anode and support is not visible but the electrolyte and porous cathode are clearly visible on the right. After sintering, the cell was reduced at 950°C in a H_2 atmosphere. The SEM micrograph (fig. 4.18) shows triple phase boundaries (tpb) at support electrolyte interface.

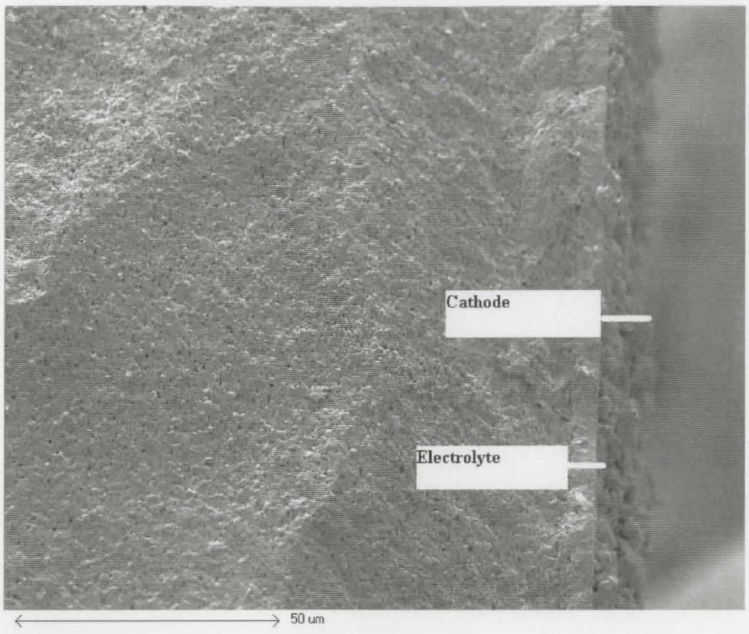

Figure 4.17 Fracture cross-section of sintered cell before reduction

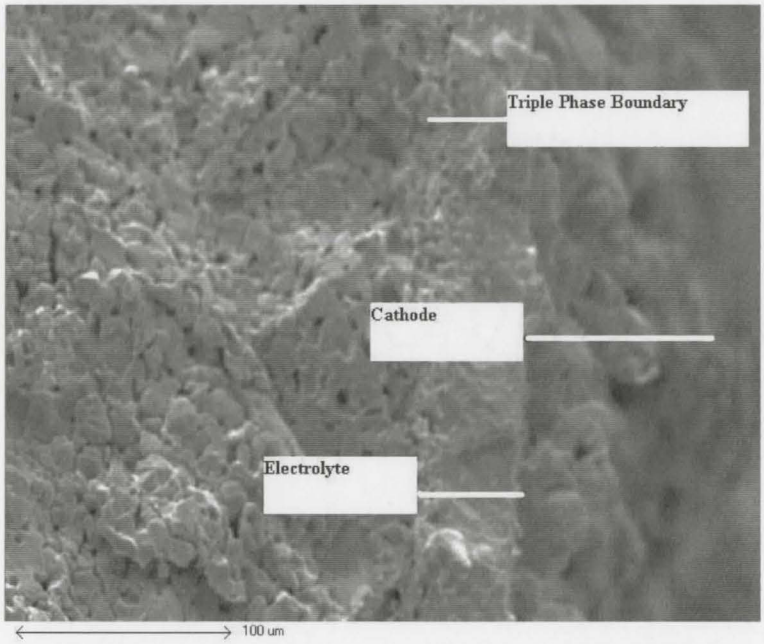

Figure 4.18 Fracture cross section of cell after reduction at 950°C for 10 h

4.3.1 Cell Performance Tests

Cell performance tests were done at 820°C with forming gas (7% H_2) as the fuel. The cells were sealed by a glass ring at 870°C. The active cell area was 0.636 cm^2 Platinum mesh was used on cathode side as a current collector. To improve conduction, one drop of cobalt sulphate solution was added to the cathode and dried prior to testing. The first results (fig. 4.19) showed an open circuit voltage (OCV) of 0.968 V and a maximum power density of 120 mW/cm^2. The second test (fig. 4.20) showed an OCV of 0.928 V and maximum power density of 80 mW/cm^2. The reduced OCV from theoretical value indicates possible leakage in the cell or surrounding seal. Nonetheless, the cell produced significant power output.

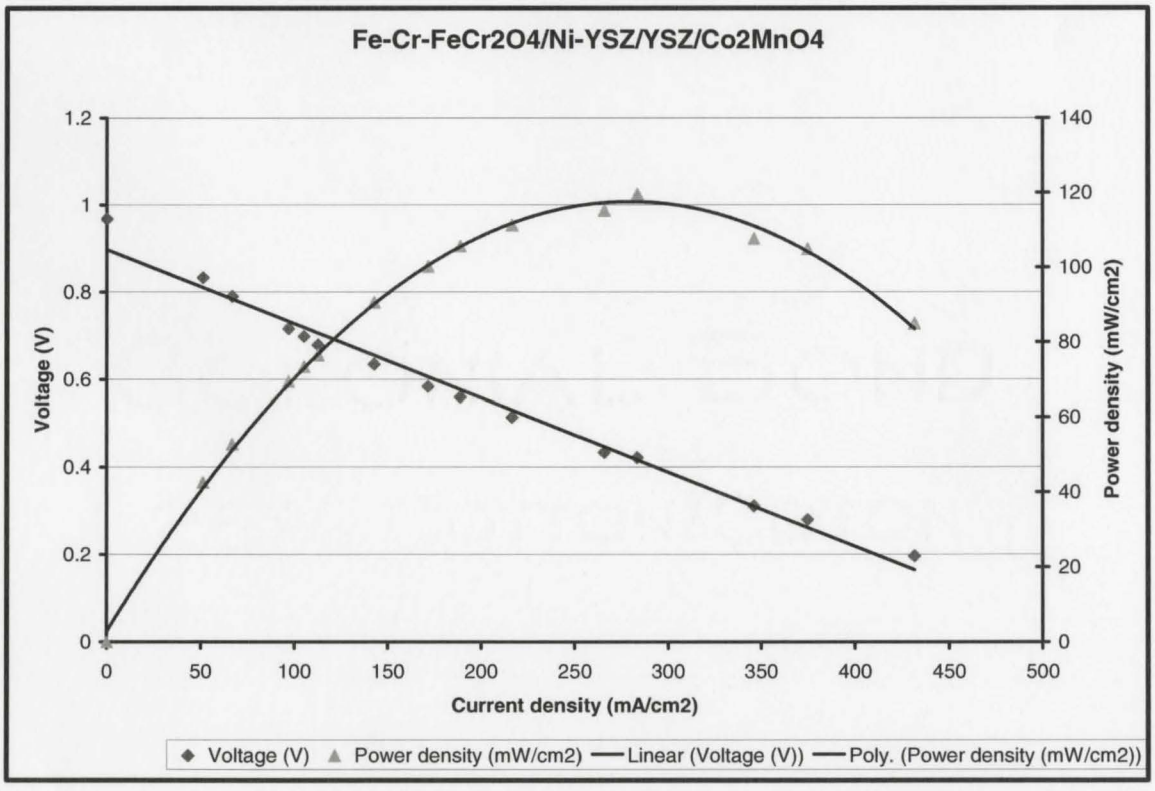

Figure 4.19 Performance of alloy supported cell with Co_2MnO_4 as cathode (Test1)

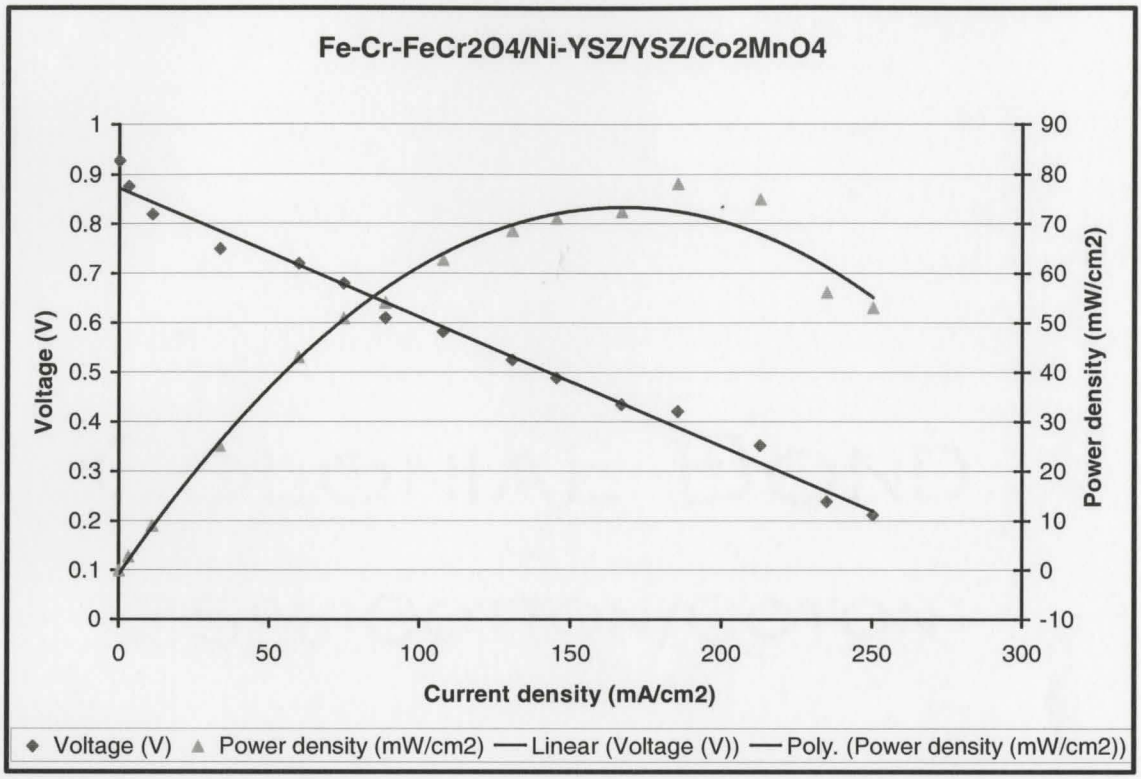

Figure 4.20 Performance of alloy supported cell with Co_2MnO_4 as cathode (Test2)

CHAPTER 5

CONCLUSIONS AND RECOMMENDATIONS

A successful fabrication process for alloy supported (metal content ~80%) SOFCs has been demonstrated. The support was fabricated from Fe_3O_4 and Cr_2O_3 oxide powders by the tape casting technique. Approximately 5% carbon was added to increase porosity in the support. Support sintering and reduction behavior was governed by powder particle size distribution and amount of carbon added. As carbon content was increased, loss in mechanical strength was observed. The kinetics of conversion of oxides into metal is fairly sluggish and therefore use of nano-grained powders of Fe_3O_4 and Cr_2O_3 at the start could increase metal content further.

Anode and electrolyte were dip coated onto the support disc. After each dip coating process, the disc was subjected to drying and binder burnout. Single step dip coating resulted in 5 to 10 micron sintered electrolyte thickness. Dip coating should be done in a controlled manner because if the thickness of the electrolyte is high, the risk of cracking and delamination increase. Another point is that in dip coating thickness of the coating is rarely uniform; therefore other techniques of coating like electrophoretic deposition (EPD), and plasma deposition could be employed.

In the present study, a new cathode material Co_2MnO_4 was used instead of conventional LSM. The cathode was screen printed on the sintered half cell and then the complete cell was subjected to drying, binder burnout, and cathode sintering. The complete cell was reduced at 950°C in H_2 atmosphere for 10 h. In reducing the sample, crack formation in the sample is a common problem. This problem can be alleviated by

switching on the reducing gas at high temperature instead of from room temperature. The sample should be put on a compatible substrate in the reaction vessel so as to avoid side reactions. Cooling rate should be sufficiently low to accommodate thermal stresses without cracking the sample.

Although power density obtained by this cell is not competitive as compared to published data with LSM cathodes, it demonstrates the viability of a metal supported cell. It is observed that after reduction, the Co_2MnO_4 cathode becomes very friable and does not properly stick to the electrolyte, thus causing a drop in power density and an increase in polarization losses. It can be solved by mixing another material with Co_2MnO_4 and the most common additive would be YSZ. The addition of YSZ would also increase the tpb length, i.e., increase the number of reaction sites.

Alternative cathodes may be considered. For example, $Cu_{1+x}\ Mn_{2-x}\ O_4$ has two times higher conductivity and a closer match in thermal expansion than $Co_2\ MnO_4$ It offers the possibility of higher catalytic activity and better cell performance.

Improved contact between cathode and current collector would enable a major improvement in performance.

REFERENCES

[1] N. Q. Minh, T. Takahashi, Science and Technology of Ceramic Fuel Cells. Elsevier, Amsterdam, 1995

[2] Steven J. Visco, Craig P. Jacobson, Igor Villareal, Andy Leming, Yuriy Matus, Lutgard C. De Jonghe, Development of low-cost alloy supported SOFCs, Electrochemical Society Proceedings, 7, 1041-1050, 2003.

[3] I. Villarreal, C. Jacobson, A. Leming, Y. Matus, S. Visco, L. De Jonghe, Metal-supported solid oxide fuel cells, Electrochemical and Solid-State Letters, 6 (9), A178-A179, 2003.

[4] B. C. H. Steele, Materials science and engineering: the enabling technology for the commercialisation of fuel cell systems, Journal of Materials Science, 36, 1053-1068, 2001.

[5] A. Boudghene Stambouli, E. Traversa, Solid oxide fuel cells (SOFCs): a review of an environmentally clean and efficient source of energy, Renewable and Sustainable Energy Reviews, 6, 433-455, 2002.

[6] http://www.eere.energy.gov/hydrogenandfuelcells/fuelcells/fc_types.html#oxide

[7] http://www.iwe.uni-karlsruhe.de/english/sofc.php

[8] http://www.che.sc.edu/centers/PEMFC/index.html

[9] K. T. Jacob, Saurabh Jain, Fuel cell efficiency redefined: carnot limit re assessed, Electrochemical Society Proceedings, V 2005-07

[10] Chunshun Song, Fuel processing for low temperature and high-temperature fuel cells challenges, and opportunities for sustainable development in the 21st century, Catalysis Today, 77, 1-2, 17-49, 2002.

[11] B. C. H. Steele, Interfacial reactions associated with ceramic ion transport membranes, Solid State Ionics, 75, 157-165, 1995.

[12] Sossina M. Haile, Fuel cell materials and components, Acta materialia, 51, 5981-6000, 2003.

[13] Hans-Heinrich Mobius, On the history of solid electrolyte fuel cells, J. Solid State Electrochem, 1, 2-16, 1997.

[14] M.L. Perry, T. F. Fuller, A historical perspective of fuel cell technology in the 20th century, Journal of the Electrochemical Society, 149(7), S59-S67, 2002.

[15] Jang J. H., Ryu J.H., Oh S.M., Microstructure of Ni/YSZ cermets according to particle size of precursor powders and their anodic performances in SOFC, Ionics, V6, n 1-2, 86-91, 2000.

[16] J. H. Lee, H. Moon, H. W. Lee, J. Kim, J. D. Kim, K. H. Moon, Quantitative analysis of microstructure and its related electrical property of SOFC anode Ni-YSZ cermet, Solid State Ionics, 148, 15-26, 2002.

[17] Hideto Koide, Yoshiyuki Someya, Toshihiko Yoshida, Toshio Maruyama, Properties of Ni/YSZ cermet as anode for SOFC, 132, 253-260, 2000.

[18] Joon-Ho Koh, Young-Sung Yoo, Jin-Woo Park, Hee Chun Lim, Carbon deposition and cell performance of Ni-YSZ anode support SOFC with methane fuel, Solid State Ionics, 149, 157-166, 2002.

[19] Rangachary Mukundan, Eric L. Brosha, Fernando H. Garzon, Sulfur tolerant anodes for SOFCs, Electrochemical and Solid- State Letters, 7(1), A5-A7, 2004.

[20] W.Z. Zhu, S.C. Deevi, A review on the status of anode materials for solid oxide fuel cells, Materials Science & Engineering, A362, 228-239, 2003.

[21] Y. L. Liu, S. Primdahl, M. Mogensen, Effects of impurities on microstructure in Ni/YSZ-YSZ half cells for SOFC, Solid Oxide Ionics, 161, 1-10, 2003.

[22] Yoshio Matsuzaki, Isamu Yasuda, The poisoning effect of sulfur-containing impurity gas on a SOFC anode: Part I. Dependence on temperature, time, and impurity concentration, Solid State Ionics, 132, 261-269, 2000.

[23] Andre Weber, Ellen Ivers-Tiffee, Materials and concepts for solid oxide fuel cells (SOFCs) in stationary and mobile applications, Journal of Power Sources, 127, 273-283, 2004.

[24] S. C., Singhal, Advances in solid oxide fuel cell technology, Solid State Ionics, 135, 305-313, 2000.

[25] S. Hashimoto, T. Shimura, H. Iwahara, Electrical properties of Ce-doped $SrMnO_3$ as a cathode material, Electrochemical Society Proceedings, V99-19

[26] Hee Sung Yoon, Dokyol Lee, Byong Ho Kim, Synthesis and characterization of $Gd_{1-x}Sr_xMnO_3$ cathode for SOFC, Electrochemical Society Proceedings, V 99-19

[27] Lutz Kindermann, Dasarathi Das, Dhirendraa Bahadur, Reinhard Weib, Hubertus Nickel, Klaus Hilpert, Chemical interaction between La-Sr-Mn-Fe-O based perovskites and Yttria stabilized zirconia, J. Am. Ceram. Soc., 80 (4), 900, 1997.

[28] E. Perry Murrey, S. A. Barnett, Improved performance in (La,Sr)MnO_3 cathodes by the addition of a Gd-doped ceria second phase, Electrochemical Society Proceeedings, V 99-19.

[29] M. Mori, T. Abe, H. Itoh, O. Yamamoto, G. Q. Shen, Y. Takeda, N. Imanish, Reaction mechanism between lanthanum manganite and Yttria doped cubic zirconia, Solid State Ionics, 123, 113-119, 1999.

[30] L. Ya. Gavrilova, V.A. Cherepanov, Oxygen nonstoichiometry and defect structure of $La_{1-x}Me_xCoO_{3-\delta}$ (Me= Ca,Sr,Ba), Electrochemical Society Proceedings, V 99-19.

[31] S. C. Paulson, Y. I. Birss, Chromium poisoning of LSM-YSZ SOFC cathodes I. Detailed study of the distribution of chromium species at a porous, single –phase cathode, Journal of the Electrochemical Society, 151 (11), A1961-A1968, 2004.

[32] K. Fujita, K. Ogasawara, Y. Matsuzaki, T. Sakurai, Prevention of SOFC cathode degradation in contact with Cr-poisoning alloy, Journal of Power Sources, 131, 261-269, 2004.

[33] T. Shibayama, T. Ishihara, M. Honda, H. Furutani, Y. Takita, Application for electrolyte of solid oxide fuel cell.

[34] Soren Primdahl, Bent F. Sorensen, Mogens Mogensen, Effect of Nickel oxide/Yttria-stabilized zirconia anode precursor sintering temperature on the properties of solid oxide fuel cells, J. Am. Ceram. Soc., 83 (3), 489-94, 2000.

[35] H. Hayashi, H. Inaba, M. Matsuyama, N. G. Lan, M. Dokiya, H. Tagawa, Structural consideration on the ionic conductivity of perovskite-type oxides, Solid State Ionics, 122, 1-15, 1999.

[36] Osamu Yamamoto, Yasuo Takeda, Ryoji Kanno, Muneyoshi Noda, Cathodic polarization phenomena of oxide electrodes with stabilized ZrO_2 electrolyte, Advances in Ceramics, V24, 1988.

[37] Wayne L. Worell, Electrical properties of mixed-conducting oxides having high oxygen-ion conductivity, Solid Oxide Ionics, 52, 147-151, 1992.

[38] Tomasz Brylewski, Makoto Nanko, Toshio Maruyama, Kazimierz Przybylaski, Application of Fe-16 Cr ferritic alloy to interconnector for a solid oxide fuel cell, Solid Oxide Ionics, V143 (2) , 131-150, 2001.

[39] W. Z. Zhu, S.C. Deevi, Development of interconnect materials for solid oxide fuel cells, Materials Science and Engineering, A348, 227-243, 2003.

[40] Hideyuki Negishi, Natsuko Sakai, Katsuhiko Yamaji, Taruhisa Horita, Harumi Yokokawa, Application of electrophoretic deposition technique to solid oxide fuel cells, Journal of the Electrochemical Society, 147(5), 1682-1687, 2000.

[41] Takeshi Yao, Akira Ariyoshi, Takashi Inui, Synthesis of $LaMeO_3$ (Me= Cr, Mn, Fe, Co) perovskite oxides from aqueous solution, J. Am. Ceram. Soc., 80 (9), 2441-44, 1997.

[42] Masashi Mori, Irreversible expansion behavior of $Mn_3O_{4+\delta}$ spinel and shrinkage behaavior of $La_{0.6}Sr_{0.4}MnO_3$ composites with the spinel during thermal cycling in O_2 atmosphere, Journal of Electrochemical Society, 149 (8), A995-A1000, 2002.

[43] Yngve Larring, Truls Norby, Spinel and perovskite functional layers between plansee metallic interconnect (Cr-5 wt% Fe-1 wt% Y_2O_3) and ceramic (

$La_{0.85}Sr_{0.15})_{0.91}$ MnO_3 cathode materials for solid oxide fuel cells, 147 (9), 3251-3256, 2000.

[44] Phillip Aitchison, Brett Ammundsen, Deborah J. James, Gary Burns, Jacques Roziere, Cobalt substitution in lithium manganate spinels: examination of local structure and lithium extraction by XAFS, Journal of Materials Chemistry, 9, 3125-3130, 1999.

[45] Rajendra N. Basu, Frank Tietz, Egbert Wessel, Detlev Stover, Interface reaction during co-firing of solid oxide fuel cell components, Journal of Materials Processing Technology, article in press,2004.

[46] Jean Duquette, Anthony Petric, Silver wire seal design for planar solid oxide fuel cell stack, Journal of Power Sources, article in the press, 2004.

[47] Q. Ming, M.D. Nersesyan, J. T. Richardson, Dan Luss, Economic production of $La_{1-x}Sr_xCrO_3$ and $La_{1-x}Sr_xMnO_3$, Electrochemical Society Proceedings, Volume 99-19.

[48] S. C. Singhal, Kevin Kendall, High Temperature Solid Oxide Fuel Cells:Fundamentals, Design,and Applications,Elsevier,2003.

[49] Richard E. Mistler, Eric R. Twiname, Tape casting theory and practice, American Ceramic Society, 2000.

[50] Courtesy Jean Duquette, Anthony Petric research group, Materials Science & Engineering McMaster University, ON Canada, 2004.

[51] K. Fujita, K. Ogasawara, Y. Matsuzaki, T. Sakurai, Prevention of SOFC cathode degradation in contact with Cr-containing alloy, Journal of Power Sources,131, 261-269, 2004.

[52] K. Fujita, T. Hashimoto, K. Ogasawara, H. Kameda, Y. Matsuzaki, T. Sakurai, Relationship between electrochemical properties of SOFC cathode and compositionship of oxide layer formed on metallic interconnects, Journal of Power Sources, 131, 270-277, 2004.

[53] Ellen Ivers-Tiffee, Andre Weber, Dirk Herbstritt, Materials and technologies for SOFC-components, Journal of the European Ceramic Society, 21, 1805-1811, 2001.

[54] Yu. V. Golikov, Izv. Akad. Nauk SSSR; Neorg. Mater., 24 (7), 1145-1149, 1988.

[55] Hangh Lingh, Masters thesis, Materials Science & Engineering, McMaster University, Hamilton, Canada, 2004

[56] F. Tietz, H.-P. Buchkremer, D. Stover, Components manufacturing for solid oxide fuel cells, 152-153, 373-381, 2002.

[57] ASM handbook for phase diagrams

APPENDIX

Slurry Composition for Fe_3O_4+Cr_2O_3 Tape Casting

Following (table A1) is the composition for the slurry for Fe_3O_4 + Cr_2O_3 tape casting having different carbon contents.

Compositions	Batch 1 (g)	Batch 2 (g)	Batch 3 (g)
Fe_3O_4	15.000	15.000	15.000
Cr_2O_3	4.967	4.910	5.013
Fish Oil	0.593	0.609	0.595
Ethyl Alcohol	7.012	7.28	7.308
Toluene	8.320	8.389	8.565
PVB	1.427	1.330	1.155
BBP	2.509	2.153	1.926
C(4023)	3.020	0.8	0.00

Table A1 slurry composition for Fe_3O_4 + Cr_2O_3 tape with varied carbon content

Slurry Composition for YSZ Tape Casting

Following table A2 is the compositions for YSZ tape casting.

Compositions	**Batch 1**	**Batch 2**	**Batch 3**
YSZ	39.995 (g)	39.996 (g)	40.040 (g)
Ethyl alcohol	9.144 (g)	9.180 (g)	9.217 (g)
Toluene	11.550 (g)	11.611 (g)	11.644 (g)
Fish Oil	0.843 (g)	0.847 (g)	0.868 (g)
PVB	2.522 (g)	2.529 (g)	2.463 (g)
BBP	5.192 (g)	5.213 (g)	4.816 (g)
Modifier (Ferro M111)	3.2 ml. (g)	3.4 ml. (g)	3.4 ml. (g)

Table A2 Constituents compositions for YSZ tape casting slurry

Slurry Composition for NiO/YSZ Tape Casting

Following (table A3) is the compositions table for NiO/YSZ tape casting.

Compositions	**Batch 1 (g)**	**Batch 2 (g)**	**Batch 3 (g)**
NiO	25.021	25.098	25.177
YSZ	15.009	15.012	15.007
C (4023)	8.072	8.001	2.024
Ethyl Alcohol	9.027	9.139	9.183
Toluene	13.5	13.656	13.708
Fish Oil	1.192	1.190	1.18
PVB	3.586	2.854	2.258
BBP	5.954	5.556	4.423

Table A3 Constituents compositions for NiO/YSZ tape casting slurry

Phases Present after 10 Hours Calcination of Fe_3O_4 + Cr_2O_3 Pellet

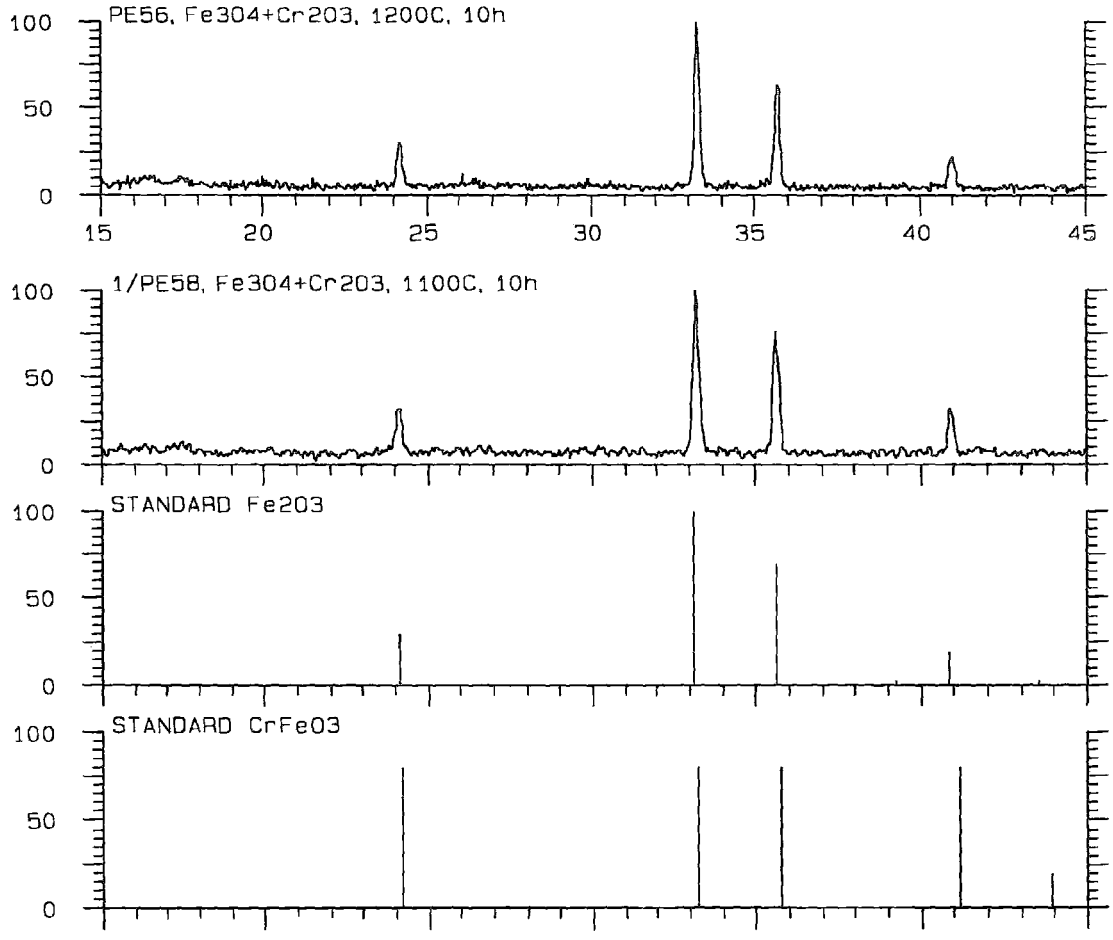

A4 XRD pattern of Fe_3O_4 + Cr_2O_3 pellet at 1100°C and 1200°C for 10 hours

TGA and DTA of Fe, Cr-$FeCr_2O_4$ Pellet

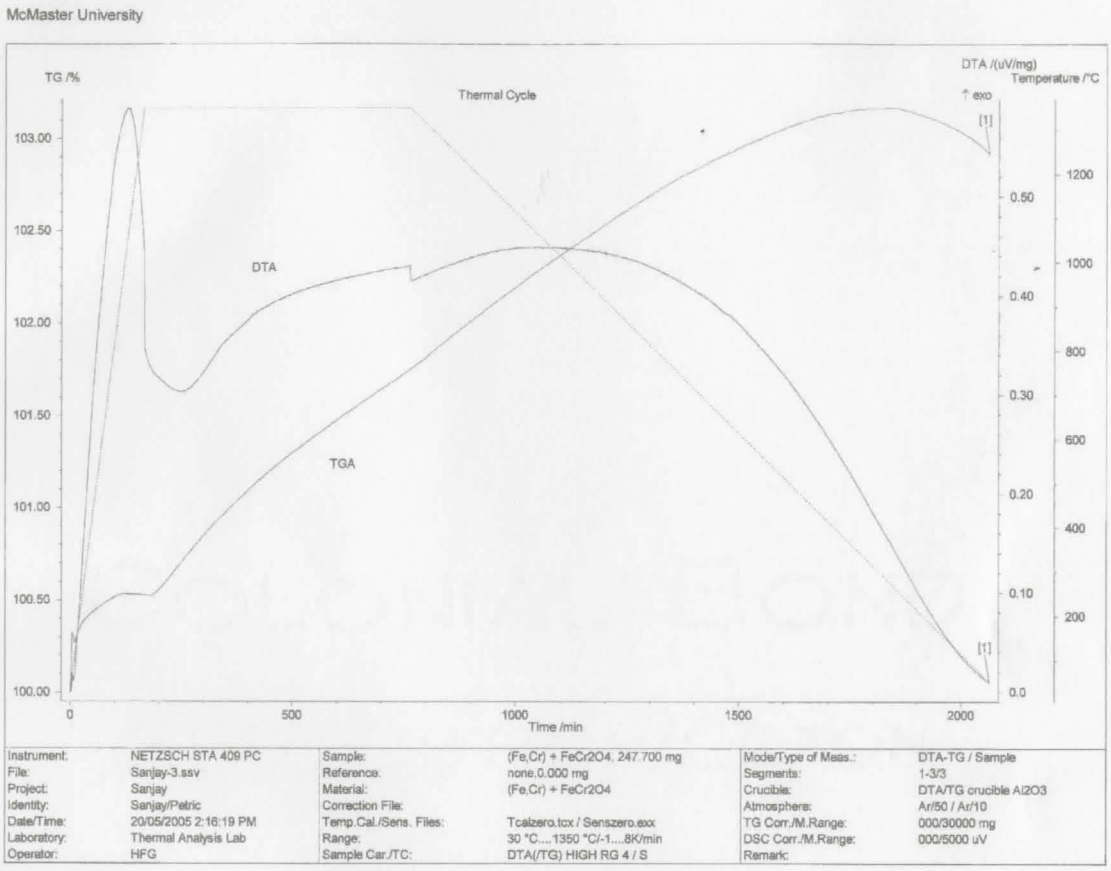

A5 TGA and DTA of reduced Fe_3O_4 +Cr_2O_3 pellet in high purity Ar atmosphere